Review

Recent Advances in Carbon Dioxide Conversion: A Circular Bioeconomy Perspective

TsingHai Wang [1], Cheng-Di Dong [2,*], Jui-Yen Lin [3,4], Chiu-Wen Chen [2], Jo-Shu Chang [3,5], Hyunook Kim [6], Chin-Pao Huang [4] and Chang-Mao Hung [2]

[1] Department of Chemical Engineering, Yuan Ze University, Taoyuan City 32003, Taiwan; thwang@saturn.yzu.edu.tw
[2] Department of Marine Environmental Engineering, National Kaohsiung University of Science and Technology, Kaohsiung City 811213, Taiwan; cwchen@nkust.edu.tw (C.-W.C.); hungcm@nkust.edu.tw (C.-M.H.)
[3] Department of Chemical Engineering, National Cheng Kung University, Tainan City 701, Taiwan; thomaslin0718@gmail.com (J.-Y.L.); changjs@mail.ncku.edu.tw (J.-S.C.)
[4] Department of Civil and Environmental Engineering, University of Delaware, Newark, DE 19716, USA; huang@udel.edu
[5] Department of Chemical and Materials Engineering, College of Engineering, Tunghai University, Taichung City 407224, Taiwan
[6] School of Environmental Engineering, University of Seoul, Seoul 02504, Korea; h_kim@uos.ac.kr
* Correspondence: cddong@nkust.edu.tw

Abstract: Managing the concentration of atmospheric CO_2 requires a multifaceted engineering strategy, which remains a highly challenging task. Reducing atmospheric CO_2 (CO2R) by converting it to value-added chemicals in a carbon neutral footprint manner must be the ultimate goal. The latest progress in CO2R through either abiotic (artificial catalysts) or biotic (natural enzymes) processes is reviewed herein. Abiotic CO2R can be conducted in the aqueous phase that usually leads to the formation of a mixture of CO, formic acid, and hydrogen. By contrast, a wide spectrum of hydrocarbon species is often observed by abiotic CO2R in the gaseous phase. On the other hand, biotic CO2R is often conducted in the aqueous phase and a wide spectrum of value-added chemicals are obtained. Key to the success of the abiotic process is understanding the surface chemistry of catalysts, which significantly governs the reactivity and selectivity of CO2R. However, in biotic CO2R, operation conditions and reactor design are crucial to reaching a neutral carbon footprint. Future research needs to look toward neutral or even negative carbon footprint CO2R processes. Having a deep insight into the scientific and technological aspect of both abiotic and biotic CO2R would advance in designing efficient catalysts and microalgae farming systems. Integrating the abiotic and biotic CO2R such as microbial fuel cells further diversifies the spectrum of CO2R.

Keywords: CO_2 conversions; abiotic processes; algal farming; biorefinery; circular bioeconomy

1. Introduction

Controlling atmospheric CO_2 concentration is essential to the mitigation of global warming. Amongst all strategies, CO_2 conversion to value-added chemicals should be a top choice. In principle, CO_2 conversion can readily take place naturally (biotic) by cultivating plants or algae to absorb CO_2 and artificially (abiotic) by using synthesized catalysts in a controlled system to accelerate electrochemical CO_2 conversion. Photosynthesis is the most known naturally occurring CO_2 conversion reaction [1]:

$$106\,CO_2 + 16\,NO_3^- + HPO_4^{2-} + 122\,H_2O + 18\,H^+ \rightleftharpoons \{C_{106}H_{263}O_{110}N_{16}P\} + 138\,O_2 \quad (1)$$
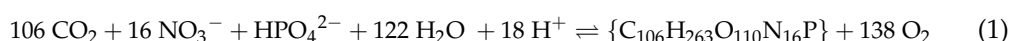
The forward and backward reaction in Equation (1) indicates the photosynthesis and the respiration, respectively. The significance of Equation (1), in addition to the

photosynthesis and natural respiration, is the involved chemical cycles of carbon, nitrogen, and phosphorus. This further implies that the reclamation of trace nutrients is an additional benefit to biotic CO_2 conversion. By contrast, artificial CO_2 conversion requires energy input since CO_2 has no heat value. Recent progress in catalysis greatly reduces the energy requirement in artificial CO_2 reduction (CO2R).

There are excellent reviews on the mechanistic aspects and effectiveness of CO2R catalysts [2–6]. Artificial CO2R can be achieved by processes, such as electrochemical [7–9], photochemical [10–12], and photoelectrochemical (PEC), by which electrons are transferred to CO_2 molecules to increase their energy content [13,14]. Electrochemical CO2R is an electron transfer reaction between the cathode and the adsorbed CO_2. Photochemical CO2R relies on the transfer of photogenerated electrons in the LUMO (the lowest unoccupied molecular orbital) of the catalyst to the HUMO (the highest occupied molecular orbital) of adsorbed CO_2. In photoelectrochemical (PEC) CO2R, the photogenerated electrons are transported to the cathode in the presence of a bias electric field. The external electric field effectively suppresses the recombination loss of photogenerated charge carriers and enhances CO2R efficiency.

In all modes of CO2R systems, catalysts (in the form of photosensitive or electric conductive) are needed to facilitate the CO_2 reduction reactions. Therefore, the stability and surface chemistry of catalysts (electrodes) become important operation parameters. For instance, it is suggested that a thin $\gamma - Al_2O_3$ overlayer could effectively stabilize the Faradaic efficiency and the partial current density of the SnO_2 catalyst in an electrochemical CO2R reaction [8]. Chang et al. (2016) have reported that photogenerated holes, not electrons, are the primary cause of instability of Cu_2O catalysts, which require Cu_2O to be operated as dark cathodes [13]. High-CO-affinity electrocatalysts (i.e., Cr, Mn, and Fe-N-C) exhibited high carbon monoxide (CO) Faradaic efficiency. The pyridinic and hydrogenated (pyrrolic) nitrogen moieties of the carbonaceous support are active sites for CO_2 adsorption [9]. Accordingly, a relatively basic surface (such as the presence of $\gamma - Al_2O_3$ overlayer and pyridinic modification) would have a positive effect on CO2R efficiency enhancement, likely through increasing the affinity of the catalyst surface toward CO_2 adsorption. Defects in a catalyst would introduce coordinately unsaturated sites (i.e., active sites for molecular chemisorption) and provide spatially supply channels for energy and electron transfers in photochemical CO2R [10]. Note that among all available CO2R processes, electrochemical CO2R is probably the simplest; therefore, it is the easiest and most sustainable (relative to chemical reduction) for operations and scaling-up.

CO2R involves the consecutive transfer of one electron or hydrogen from the catalyst to CO_2 and intermediates, which gradually reduces the carbon oxidation number stepwise. Only intermediates that possess even oxidation numbers are thermodynamically stable. This is why formic acid (FA, HCOOH), carbon monoxide (CO), formaldehyde (HCOH), methanol (CH_3OH), and methane (CH_4) are always found in CO2R reactions. This review focuses on recent advances of CO2R systems, both biotic and abiotic processes, and as far as the broad view of CO_2 conversion is concerned, three significant implications are noted [15].

Mitigating greenhouse gas effect: Electrocatalytic CO2R is usually conducted with high-purity CO_2 based on thermodynamics considerations. This means that additional electricity is required for concentrating CO_2 feedstock; however, the majority of electricity in modern society is produced through fossil fuels. Adopting electrocatalytic CO2R for the mitigation of the greenhouse effect would instead increase atmospheric CO_2 concentration [2,16]. Therefore, increasing the deployment of renewable energy would be equally important in addition to the efficiency improvement of electrocatalytic CO2R from the prospect of greenhouse gas mitigation.

Electrochemical conversion of CO_2 to fuels: In order to achieve a carbon neutral footprint through electrocatalytic CO2R, produced hydrocarbons should not be fed to the combustion engines directly. Instead, they should be feed for fuel cells [15]. Again, increasing the efficiency of fuel cells for feeding CO_2-derived methanol [17,18] or formic

acid [19,20] is another issue of concern. Selectivity of CO2R catalysts is crucial too as it minimizes the carbon footprint required for subsequent separation and concentration of hydrocarbons produced from electrocatalytic CO2R [21].

Electrochemical conversion of CO_2 to a building block: Electrocatalytic CO2R to carbonaceous fuels usually leads to a positive carbon footprint as mentioned above. However, a carbon neutral footprint could be possibly reached by converting CO_2 to a building block as an alternative. This is because CO_2 is a C1 building block that requires no extra energy for its production [22]. For example, carbon monoxide produced by electrocatalytic CO2R could be directly used as the source for producing phosgene [23,24]. Similarly, as-obtained methanol and formic acid could be feedstocks for reversible chemical hydrogen storage and other applications [5,25].

Apparently, converting CO_2 to a building block for chemicals production could entice the pursuant of electrocatalytic CO2R. Indeed, all conceptual designs of an economically affordable CO2R business for achieving a negative carbon footprint have assumed that the CO2R catalysts could exhibit excellent reactivity and selectivity. For instance, Gai et al. (2016) performed a conceptual design of methanol production from CO_2 at an industrial scale using ASPEN Plus® (Bedford, MA, USA) in which CO and H_2 are produced from the electrolysis of CO_2 and H_2O [26]. They found that when CO_2 conversion is less than 42%, the optimal methanol synthesis route is CO hydrogenation. Importantly, the achievement of a near zero carbon emission power plant is strongly built on the assumption that CO is the only intermediate and no additional energy is required for CO isolation [26]. Sun et al. (2019) have developed a 20 MWth solar–wind biodistributed energy system for simultaneously biomass cascade utilization, water resource conservation, waste heat recovery, and CO_2 mitigation for hydrogen, formic acid, and grapheme production [27]. Again, in their framework, the energy efficiency is vulnerable to the compromised selectivity of electrocatalytic CO2R. Based on the above considerations, it is clear that the success of a CO2R industry strongly relies on multidiscipline cooperation and that technology is part of this. Additional bonuses such as creating jobs, building blocks for chemicals, and carbon right trading would make CO2R more sustainable. Integrating the knowledge of biotic and abiotic CO2R is another useful approach. A good example is the microbial electrosynthesis system (MES), in which the microbial is responsible for biotic CO2R, while engineering the electrode (abiotic CO2R) further improves the overall CO2R efficiency. Accordingly, recent advances in abiotic CO2R and biotic CO2R will be reviewed herein. Having a deep insight into the scientific and technological aspects of both abiotic and biotic CO2R would advance the design of efficient catalysts and the microalgae farming system. We first focus on the technology aspect of abiotic CO2R by discussing the reactivity and selectivity of CO2R catalysts and reaction mechanisms in both water and gas phases. The effect of the surface chemistry of synthesized catalysts on the reactivity and selectivity of CO2R will be addressed. This will be particularly beneficial to the rational design of high-efficient catalysts for CO2R conversion. CO2R through microalgae abstraction of CO_2 is highly influenced by the bioactivity of selected microalgae. Separation and purification of various value-added chemicals obtained is another issue of concern, and further refinery of algal biomass is also included in this review. Additional considerations such as the involvement of other stakeholders that allow CO2R to be more sustainable are also discussed.

2. CO_2 Conversion Processes

2.1. Homogeneous Catalysts for CO2R

Figure 1 illustrates the different reaction steps involved in the homogeneous and heterogeneous CO2R. In the homogeneous CO2R system, two reaction steps are suggested: (i) the redox of the catalyst and (ii) the charge transfer from the catalyst to CO_2. The homogeneous CO2R catalyst is also known as the molecular catalyst and is designed by mimicking the structure of chlorophyll. In the chlorophyll structure, both the metal center (Lewis acid) and the chelating ligand (Lewis base) are known to have a strong influence on the energy gap and electron transfer pathway [12]. For example, the porphyrin

(in porphyrin-Co, porphyrin-Cu, and porphyrin-Au homogeneous catalysts) has been identified as both a ligand and a photoswitch to regulate the electron transfer pathway to the metal center [12]. An important feature of the homogenous catalyst for CO2R is that CO_2 reduction occurs at the potential of the catalyst, not at the thermodynamic potential, where the CO_2 reduction takes place [2]. Accordingly, the mass transport of homogeneous catalysts from the diffusion layer to the electrode surface therefore regulates the CO2R efficiency. It is difficult to conclude whether either homogeneous or heterogeneous CO2R reduction is advantageous over the other. The CO2R efficiency in the continuous operation unit of the flow cell will be high over homogeneous catalysts. However, surface engineering at a heterogeneous catalyst for enhancing CO2R selectivity is relatively easy. The sluggish oxygen evolution kinetics occurring at an anode (as it involves a four-electron transfer) limits the overall CO2R efficiency [28].
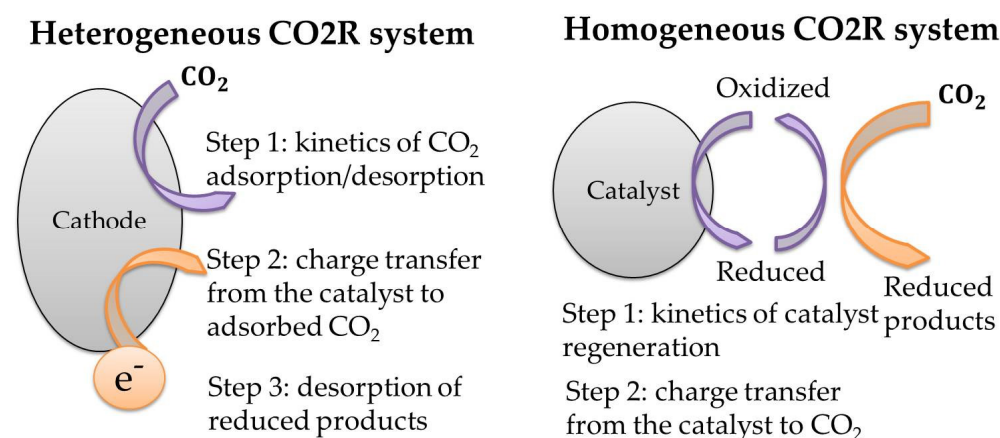

Figure 1. Electrochemical CO2R in heterogeneous (**left**) and homogeneous (**right**) catalyst systems.

2.2. Heterogeneous Catalysts for CO2R

In the heterogeneous CO2R system, three reaction steps are involved: (i) CO_2 adsorption at the catalyst surface; (ii) charge transfer from the catalyst to adsorbed CO_2; and (iii) desorption of reduced products. The important CO2R intermediate in this system is the highly reactive CO_2^- radical anion, which is produced through reorganizing linear CO_2 to the bent radical anion [29]. Apparently, bending linear CO_2 requires significant amounts of additional energy to form/break chemical bonds (chemisorption) and transfer electrons. Accordingly, kinetics in bond-forming interactions and electron transfer significantly regulate CO2R efficiency. The distribution of CO2R products is further identified to be closely influenced by the activation energy of chemisorption [2–4]. For example, the activation energy of metallic catalysts, such as Pt, Ag, and Cu for CO_2 chemisorption is relatively low. This accounts for the fact that CO is the major product in this case as CO_2 reduction is initialized by the charge transfer from the catalyst surface to the adsorbed CO_2 [30]. By contrast, hydrogen transfer would be the dominant reaction in CO2R if the activation energy for CO_2 chemisorption is relatively high. This explains that the CO2R through Cu cathode mainly produces hydrocarbons, methanol, and formaldehyde [31]. Nanostructured catalysts are frequently used in heterogeneous CO2R because of the large specific surface area, which always comes with a great fraction of highly active low-coordination sites, such as edges, steps, and defects [32]. Composite CO2R catalysts, such as metal–metal oxide, metal–carbon, and others will exhibit synergistic effects as they accelerate reaction kinetics, enhance catalyst stability, and improve selectivity relative to their individual counterpart [3].

3. The Chemistry of Abiotic CO2R

3.1. Abiotic CO2R in Water Phase

CO2R can occur in the water or gas phase. In the former system, carbonate species, namely, $H_2CO_3^*$, HCO_3^-, CO_3^{2-}, are reduced. In the latter, gaseous CO_2 is reacted with

electron donors over catalysts and C1 or C2 compounds such as CO, formate, methanol, and oxalate are major products. Undoubtedly, the usage of rare and precious metals, such as Re and Pd, always leads to the highest CO2R efficiency [4]. The application of transition metals such as Fe, Mn, and Ni has received much attention recently because of material abundance and economical affordability [33,34].

3.1.1. Effect of Cu Surface Chemistry on Abiotic CO2R

Buckley et al. (2019) have studied the structure-reactivity relationships of electrocatalytic CO2R on modified Cu cathode surfaces [35]. The Cu cathode is first modified with long chain hydrocarbons so as to render the Cu surface hydrophobic. Modified electrodes are used to study the CO2R reaction in CO_2-saturated $KHCO_3$ (0.05 M) solution [36]. The Faradaic efficiency (η_F) of each species is calculated by Equation (2):

$$\eta_F = \frac{nFVC}{Q} \tag{2}$$

where F is the faraday constant (96,485 C-mol^{-1}), V is the volume of electrolyte (specifically the catholyte), C is the concentration of carbonate species (M), and Q is the total charge passing through the cathode during electrocatalysis CO2R. n is the number of electron transfer in the CO2R process. For example, n = 2 for CO_2 reduction to CO or HCOOH (FA). The partial current density (j_i) of certain species is the product of the Faradaic efficiency and total current density (j_{total}):

$$j_i = \eta_F \times j_{total} \tag{3}$$

Figure 2 shows the replotted contour image of the current density of FA, CO, and H_2 production in electrocatalytic CO2R over the modified Cu cathode [35]. Two interesting features are noted in Figure 2. First, FA is the major CO2R species on Cu-based cathodes as its value is about tenfold higher than that of CO. Second, the hot zone (the red area) of the hydrogen current occurs at the left-handed side of the figure that corresponds to the region with the lowest CO current. This clearly indicates that electrocatalytic hydrogen production profoundly competes with CO evolution. Importantly, the hot zone of hydrogen evolution appears in the region with a moderate FA current (0.5~2.5 mA/cm^2). This means that FA formation is less affected by hydrogen evolution than that of the CO formation [13]. It must be mentioned that increasing operation potential inevitably leads to high H_2 yield (Figure 3) [37]. Due to thermodynamics restrictions, FA and CO evolution in CO2R is suggested to be carried out at a relatively low potential condition.

Engineering electrochemical properties of cathode materials enhances the selectivity. Designing an efficient catalyst for CO2R is a highly technical challenge due to the strong completion from the hydrogen evolution reaction (HER) [3]. Factors such as catalytic reactivity, product selectivity, Faradaic efficiency, catalytic stability, and reduction mechanisms are crucial to controlling the efficiency of CO2R [38]. A systematical evaluation of the effect of catalyst structure on reaction selectivity is hence highly desirable [4]. Taking the electrocatalytic CO2R molecular system as an example, the energy required to dissociate an M–H bond to form a hydride is the key parameter in CO2R selectivity [2,4,39,40]. Figure 4 shows pathways regulating the transfer of either two protons (for CO evolution) or two electrons (for formic acid formation) and in both cases hydrogen evolution is always the major competitive side reaction.

In this framework, the preferential interaction between the catalytic metal center and CO_2 over protons is responsible for the selectivity for CO evolution. While the moderate hydricity facilitates CO_2 insertion into M–H bonds for FA production, strong hydride donors catalyze H_2 formation [2,4,39,40]. It has been suggested that catalytic activity requires the presence of a weakly coordinating solvent molecule that can readily become dissociated during the catalytic cycle as to provide a vacant coordination site for water binding and assisting C−O bond cleavage [4]. Generally, H_2 and FA formations are favorable reactions in aqueous solutions [39]. In fact, by plotting the hydricity as a function of individual free

energy for the one-electron reduction of the parent species, a linear correlation appears indicating high FA selectivity over CO formation. Importantly, this correlation extends over a wide range of metals, ligand architectures, structural geometries, and overall charge of the metal hydride [40]. High overpotential is always found in CO2R [41]. Despite hydrogen evolution always being a competing reaction in CO2R, it is still worthy of scientific investigation on the hydrogenation of CO_2 to FA and dehydrogenation of FA as a practical hydrogen storage pathway [5]. FA formation essentially increases the density of hydrogen gas [6]. This opens a practical alternative, such as the direct formic acid fuel cells (DFAFC) [42]. Major heterogeneous metal catalysts, such as In, Sn, Hg, and Pb exhibit high FA selectivity [5,6,41,42]. Electrochemical CO2R on polycrystalline Sn surfaces exhibits high FA selectivity too. Formation of *OCHO at Sn surfaces is the key intermediate for FA production due to optimal *OCHO binding energy. The results suggest that oxygen-bound intermediates are critical to understanding the mechanism of CO_2 reduction to HCOO– on metal surfaces [43].
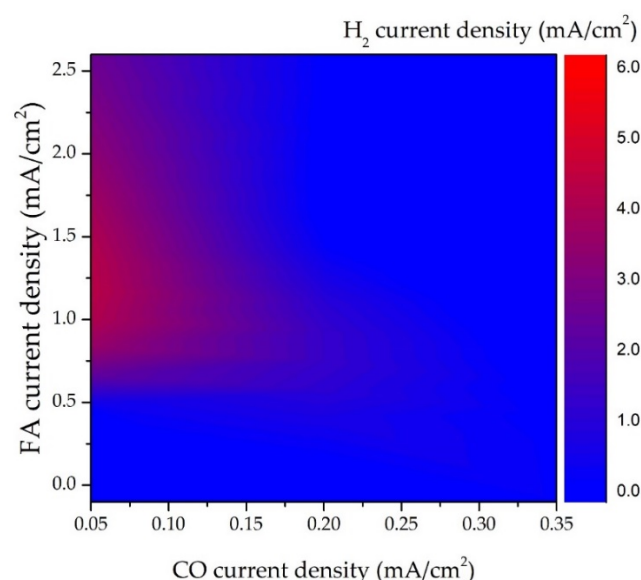

Figure 2. Current density of FA, CO, and H_2 production in electrocatalytic CO2R over modified Cu electrode. Replotted data from Buckley et al. (2019) [35].

Cu is known to have relatively low CO selectivity because the CO produced is further reduced to several multi-carbon oxygenates (i.e., ethanol, acetate, and n-propanol) [41]. Specifically, sulfur-modified copper catalysts (Cu–S) exhibit positive correlation between particle size and selectivity toward FA evolution [44]. Nanostructured porous dendritic Cu-based catalysts show stable and selective conversion of CO_2 into FA at high current density with low overpotential [45]. The relatively low CO selectivity on Cu surfaces results from consecutive CO electroreduction activity [46]. That is, in CO_2-saturated aqueous solutions, polycrystalline Cu catalysts produce a mixture of compounds. Indeed, H_2 evolution is dominated at low overpotential, CO and FA formation mainly occurs at high overpotential, while hydrocarbons, ethanol, acetate, and n-propanol formation happen at the most extreme overpotentials [47,48]. In a CO_2 free environment, CO is reduced to hydrocarbons and multi-carbon oxygenates over the Cu catalyst [49,50]. Interestingly, oxide-derived Cu (Cu catalysts prepared by reducing Cu_2O) shows much higher H_2 selectivity than polycrystalline Cu [51]. Similarly, aqueous electrochemical CO reduction to C2 products by face-to-face coordinated thiol-terminated metalloporphyrins on copper electrodes exhibits 83% Faradaic efficiency and 1.34 mA/cm^2 current density at −0.40 V vs. RHE. This is a significant improvement in both selectivity and activity by one order of magnitude over parent copper surfaces or copper functionalized with porphyrins in an edge-on orientation [52]. In a similar system, oxide-derived copper (OD-Cu) electrodes

exhibit a high CO reduction performance by producing ethanol and acetate with >50 % Faradaic efficiency at −0.3 V vs. RHE [53].
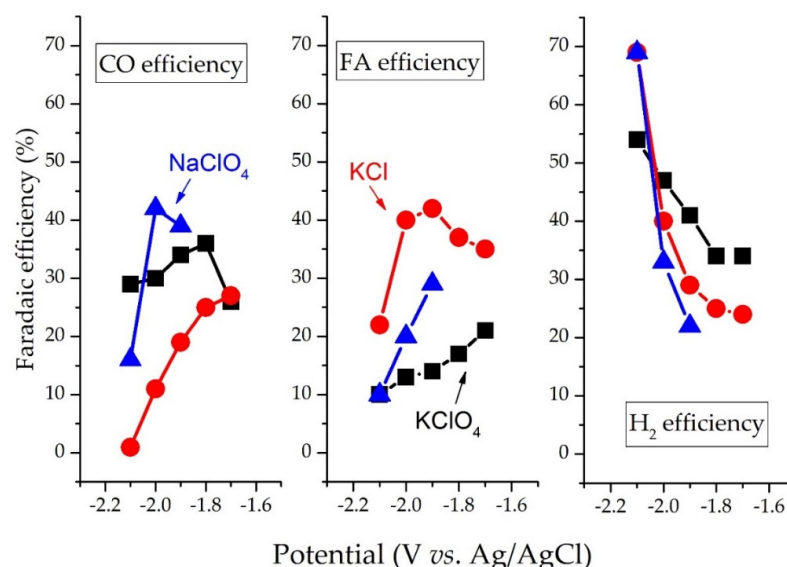

Figure 3. Faradaic efficiency of CO, FA, and H_2 production in electrocatalytic CO2R over boron-doped diamond (BDD) cathodes as a function of operation potential. Replotted data from Tomisaki et al. (2019) [37].
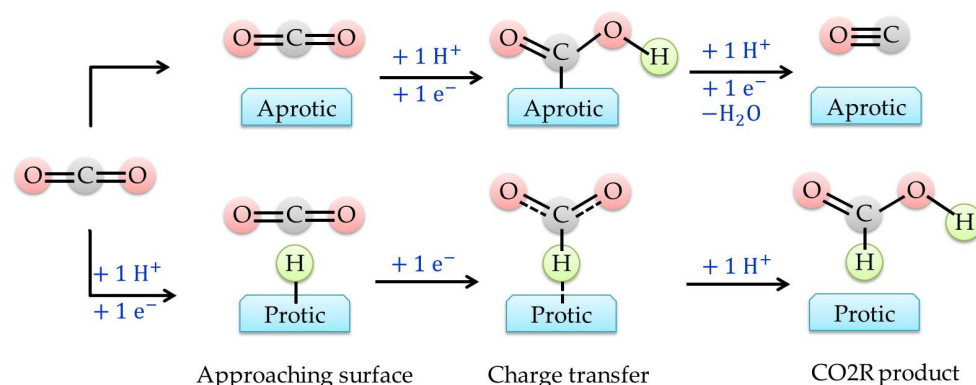

Figure 4. Illustration of CO2R pathways occurring at the protic and aprotic surface. Rearranged from Buckley et al. (2019) [35].

In a short summary, the selectivity of abiotic CO2R in the aqueous phase is highly sensitive to the surface chemistry of Cu-family catalysts. CO2R occurring at the aprotic surface tends to yield CO as the major product. By contrast, CO2R happening at the protic surface is prone to produce hydrocarbons and multi-carbon oxygenates as the major products. In this case, the selectivity is strongly affected by the involved reaction pathway. In the former case, the reduction is achieved through the charge transfer, while in the latter case the hydride transfer is mainly responsible for the CO2R. The adsorption affinity between reduced intermediates and Cu-family catalysts is another critical factor regulating the CO2R selectivity. High adsorption affinity slows the desorption of the reduced intermediates, which enables their consecutive reduction. This explains that the hydrocarbons and multi-carbon oxygenates as the major products are found in this case. It is thus concluded that increasing CO2R selectivity could be achieved through the modification of surface hydrophobicity and adsorption affinity.

3.1.2. Effect of Surface Chemistry of Non Cu-Family Catalysts on Abiotic CO2R

In the iron-based CO2R, introducing the extra elemental Fe plate profoundly decreases the overpotential of the microbial electrosynthesis system (MES) [54]. In this MES system,

all produced CO_2 is reduced to formate at the cathode and vast hydrogen is produced during the digestion of waste activated sludge. This is attributed to the high selectivity toward formic acid evolution over CO and methane production to the reduction of H^+ at the cathode due to the slow methanogensis in Fe-C MES [54]. In the case of photocatalytic CO2R, enhancing sunlight conversion efficiency is always accompanied with improving CO2R selectivity [55]. Similar to the strategy adopted in the dye-sensitized photoelectrochemical cells [56], increasing selectivity in FA formation is usually achieved through coordinating active metals with covalent organic frameworks. For example, the columnar orientation COFs (covalent organic frameworks) provides a high-efficient charge carrier transport through the ordered π-electronic pathway, which improves electron transfer from COF to metal moiety and thus increases the reactivity [55]. The results of density functional theory computations further reveal that COFs decorated with electron-donating substituents favor CO_2 reduction by decreasing the hydricity of the Rh–H bond. This results in a lower hydride transfer barrier toward formic acid production [57] because the selectivity toward CO or HCOOH production is dependent on the coordination environment of the metal ion being capable of cleaving the C–O bond in the metal–CO_2H intermediate [55]. Specifically, an electron-rich coordination environment breaks the $C-O$ bond to form CO, whereas an electron-deficiency coordination environment tends to enhance the $C-O$ bonding thereby enhancing FA formation [58]. That is, if the center metal in covalent-organic frameworks (COFs) is a strong π-donor, such as Co(II), it usually tends to promote CO evolution. By contrast, a weak π-donor, such as Zn(II), favors HCOOH production [55]. A catalyst exhibiting low adsorption energy for HCOO* (i.e., a large energy difference between the two adsorbed CO_2 reduction intermediates, namely HCOO* and COOH* and large H* adsorption energy) would have high FA selectivity [59]. Ajmal et al. (2019) have studied the selectivity of the CO_2 reduction reaction over bimetallic CuZn alloy catalysts and reported that the Faradaic efficiency and partial current density of FA on $Cu_{0.5}Zn_{0.5}$ (equal molar ratio of Cu and Zn) are enhanced by nearly 4 and 5 times, respectively, that of Cu foil [60]. The high selectivity of the CuZn bimetallic alloy catalyst is originated from the synergistic effect of Cu and Zn. In this case, the Zn (a weak π-donor) is likely to create a large energy difference for the adsorption of two CO_2 reduction intermediates, namely, HCOO* and COOH*. An et al. (2019) have studied CO_2 reduction over Sn/SnOx catalysts and reported a maximum FA Faradaic efficiency of 89% at -1.7 V (vs. Ag/AgCl) in a 0.1 M CO_2-saturated $KHCO_3$ solution [61]. The authors further concluded that Sn(IV) and Sn(II) species are mainly responsible for controlling the overpotential and suppressing H_2 evolution toward improved FA selectivity. Chatterjee et al. (2019) have reported that nanoporous Pd-based alloys (np-PdX, X = Co, Ni, Cu, and Ag) exhibit FA selectivity following the order: np-PdAg > np-PdCu > Pd/C > np-PdNi > np-PdCo [62]. They have concluded that the composition-dependent behavior was governed by CO adsorption strength associated with the presence of transition metal alloying components near the Pd-skin surface and a composition-dependent change in the near surface H-sorption capacity. Interestingly, the free-standing np-PdCo and np-PdNi catalysts are able to sustain a high formate partial current density (>20 mA-cm^{-2}) with high CO poisoning tolerance while exhibiting insignificant loss of the active area [62]. This further highlights the importance of durability and resistance of catalysts against CO poisoning during CO2R.

The results of computational hydrogen electrode model simulation reveal a striking similarity in CO2R electrocatalytic activity for the Cu_3 vs. Cu_5 and Cu_4 vs. Cu_6 size-selected clusters [63]. The rate-limiting potential of Cu_4 and Cu_6 clusters in CO2R is the proton-electron ($H^+ + e^-$) transfer to CO* (species adsorbed on clusters) to form CHO*, which is also the rate-limiting step on Cu surfaces. On the other hand, with respect to Cu_3 and Cu_5 clusters, removing OH* from the cluster surface (OH* $\rightarrow$ S + OH) is the rate-limiting step in CO2R [63]. The above simulation unambiguously implies the role of surface defects, in addition to bulk electrocatalysts, in regulating CO2R reaction pathways. Indeed, the electrolysis of CO_2 on 4-aminomethylbenzene-modified Pb electrodes exhibits a current density as high as 24.0 mA/cm^2 (at -1.29 V vs. RHE) and a FA Faradaic efficiency

greater than 80% [28]. Pt-based alloys having high-index facets generally show high specific catalytic activity over those having low-index facets [64]. Exposing the high-index facets of nanosized particles is promising to enhance Pt utilization and at the same time enriches crystalline defects in the CO2R catalyst [64]. Similarly, Pan et al. (2019) have reported that N,S-codoped carbon catalysts exhibit 92% CO Faradaic efficiency and CO current density of 2.63 mA/cm^2 at a low overpotential of 0.49 V versus RHE [65]. Incorporating S in N-doped carbon introduces a high population of activate pyridinic N sites, which significantly decreases the free energy barrier for the formation of intermediate *COOH thereby enhancing CO adsorption toward high CO selectivity [65]. The high CO selectivity of the $Pd_{85}Cu_{15}$ catalyst is attributed to the presence of a larger number of low-coordination Cu sites than active monometallic Pd sites on the catalyst [66]. Accordingly, manipulating the size and chemical composition of bimetallic nanoparticles is critical to the selectivity of CO2R [66]. Results of density functional theory calculation indicate that high reactivity and selectivity are the outcome of defects that stabilize the *OCHO intermediate [67]. Surface modification of the Cu catalyst with protic, hydrophilic, and cationic hydrophobic species results in increasing the selectivity of H_2, FA, and CO, respectively [35]. Table 1 summarizes the performance of various CO2R processes. Note that Faradaic efficiency alone is not sufficient to express the degree of selectivity because the current density of individual species is also an important characteristic of an efficient catalytic CO2R reaction. In addition, as mentioned above, a low faraday efficiency in CO/FA is usually accompanied by a high faraday efficiency in H_2 evolution, which is another valuable product of CO2R in the aqueous solution.

Table 1. Summary of CO2R performances included in this study.

Base of Catalyst	FE (%) in FA	CO2R Condition	Reference
Cu modified with polymeric	38–45	-0.7 V_{RHE} in 0.05 M K_2CO_3 and 4 mM KCl with 5 sccm CO_2	[35]
boron-doped diamond	~70	-2.1 V (vs. Ag/AgCl) in KCl aqueous solution	[37]
polycrystalline Sn	~70	-1.0 V_{RHE} in 0.1 M $KHCO_3$ with 20 sccm CO_2	[43]
sulfur-modified copper	~80	-0.8 V_{RHE} in 0.1 M $KHCO_3$ with 20 sccm CO_2	[44]
Cu	~85	-1.6 V vs. ferrocenium voltage in CO_2-saturated $[EMIM](BF_4)/H_2O$ (92/8 *v/v*) ionic liquid solution	[45]
Cu (1.5 cm × 3 cm)	~20	-0.8 V_{RHE} in 0.1 M $KHCO_3$ with 20 sccm CO_2	[47]
Cu	~20	-1.4 V_{RHE} in 0.5 M KCl with 70 sccm CO_2	[48]
$Cu_2O@Cu$	~40	-0.7 V_{RHE} in 0.1 M $KHCO_3$ with 5 sccm CO_2	[51]
Iron-graphite electrode pair	~18	-0.6 $V_{Ag/AgCl}$ with CO_2 saturated 0.5 M$NaHCO_3$ in anaerobic sludge digestion process	[54]
Co incovalentorganic frameworks	1.02 mmol $h^{-1}g^{-1}$ in CO	MeCN with triethanolamineas sacrificial reducing agent and $Ru(bpy)_3Cl_2$·asphotosensitizerunder simulated sunlight	[55]
$In_{0.6}Bi_{0.2}Sn_{0.2}$ alloy on a halide perovskite	~95	-1.3 V_{RHE} in 0.5 M $KHCO_3$ with 20 sccmCO_2under simulated sunlight	[59]
$Cu_{0.5}Zn_{0.5}$	~60	-1.3 V_{RHE} in CO_2 saturated 0.1 M $KHCO_3$ under simulated sunlight	[60]
SnOx/Sn	~80	-1.7 $V_{Ag/AgCl}$ in 0.1 M CO_2-saturated $KHCO_3$	[61]
$Pd_{15}Ni_{85}$	~50	-0.5 V_{RHE} in 1.0 M CO_2-saturated $KHCO_3$	[62]
Pb modified with 4-aminomethylbenzene	~80	-1.3 V_{RHE} in 1.0 M CO_2-saturated $KHCO_3$	[28]
N,S-codoped carbon catalysts	~90 in CO	-0.6 V_{RHE} in 0.1 M $KHCO_3$ with 34 sccm CO_2	[65]
$Pd_{85}Cu_{15}$/C	~86 in CO	-0.9 V_{RHE} in 1.0 M CO_2-saturated $KHCO_3$	[66]
defective β-Bi_2O_3 double-walled nanotubes	~90	-0.8 V_{RHE} in 0.5 M $KHCO_3$ with 20 sccm CO_2	[67]
3.7 nm Pd nanoparticles	~90 in CO	-0.9 V_{RHE} in 1.0 M CO_2-saturated $KHCO_3$	[68]
boron-doped Pd catalyst	~70	-0.5 V_{RHE} in 1.0 M CO_2-saturated $KHCO_3$	[69]

Electrolytes also play a crucial role in determining CO2R selectivity. CO2R over the BDD electrode in the $KClO_4$ electrolyte produces CO, whereas FA is the major prod-

uct in the KCl electrolyte. This is because ClO_4^- promotes the adsorption of $CO_2^{\bullet -}$ intermediates [37]. Similarly, Eder et al. (2019) have reported that on Ru-based catalysts, hydrosilanes additives and KF stabilized formate intermediates (silylformate) forms form potassium formate with a turnover number of 110 mmol-formate/mmol-Ru [70]. Note again that the CO2R selectivity is a function of applied voltage, which gradually shifts from $HCOO^-$/HCOOH to CO/H_2 with increasing overpotentials [68,69]. Based on the above consideration, a new approach for effective CO2R by an aluminum hydride-like reductant has been attempted [71]. The reductant is an organoaluminum complex containing a formal aluminum double bond (dialumene). Weetman et al. (2019) have demonstrated that dialumene improves the selective formation of formic acid equivalent via the dialuminum carbonate complex rather than the conventional aluminum–hydride-based cycle [71]. Likewise, Zhao et al. (2019) have reported that the KBH_4 reduces CO_2 to HCO_2^- readily, accompanied by the release of activate intermediate species and H^+. Further, CO2R is accelerated by a Cu/Ni bimetal catalyst that effectively regenerated the active boron species [72].

Briefly, the surface chemistry of non-Cu-family catalysts also strongly influences the selectivity of abiotic CO2R in the aqueous phase. Unlike the Cu-family catalysts, the unique characteristics of non-Cu-family catalysts is that they can be tailored with a specific porous framework. In this configuration, the kinetics in the confined space govern the CO2R selectivity. The localized coordination environment is another factor regulating the overall CO2R selectivity, which can be modified via doping or introducing defects. Along with the modification is the adjustment in the energy levels that further affects the lifetime (stability) of the COR2 intermediate and consequently the CO2R selectivity.

3.2. The Chemistry of Gaseous Phase Abiotic CO2R

Several valuable chemicals such as CO, methane, methanol, low olefins, and long-chain carbohydrates could be produced from the gaseous phase CO2R reaction. To achieve selective CO2R, catalysts that are effective in activating both H_2 and CO_2 and stabilizing surface intermediates are needed. To this end, most catalysts are comprised of metallic sites, which are active in splitting adsorbed H_2 (from H_2 to H*) and exhibit a high affinity toward CO_2 adsorption. Additional modification with alkali or noble metals can further change the surface acidity or aid in the formation of an extra alloy phase in the catalyst [73]. The metal/support interfacial sites are highly active in CO_2 hydrogenation due to electron perturbation of the metal and partial reduction of metal oxide via the H-spillover mechanism [74,75].

Wet impregnation and co-precipitation are the two most frequently used methods to synthesize heterogeneous catalysts for CO_2 hydrogenation [76,77]. Nanosized catalysts can be synthesized by flame-spray pyrolysis [78]. The catalysts made by pyrolyzing metal organic precursors can achieve a complex nanostructure with high surface metal loadings [79,80] and the carbon sites can promote the adsorption and activation of CO_2 [81]. Fixed bed reactor configuration is applied in the evaluation of catalytic performance, in which specific amounts of catalysts are distributed over inert particles, such as SiC or silica, to the minimize hot spot phenomenon. After pre-reduction of the catalysts in H_2 flow, the stream that contains certain ratios of H_2/CO_2/inert gas with a specific gas hourly space velocity (GHSV) is injected into the fixed bed reactor. The CO_2 conversion (X_{CO2}) and selectivity (S) toward CO and low hydrocarbons are measured from on-line gas chromatography, while the long chain hydrocarbons are collected in a cold trap for further quantification.

3.2.1. Hydrogenation of CO_2 to CO and CH_4

Under ambient pressure, hydrogenation of CO_2 over most metal catalysts produces either CO or CH_4. The product CO can serve as a feedstock in the methanol synthesis process and the Fischer–Tropsch process for further carbohydrate synthesis [73]. Conversion of CO_2 to methane could buffer the fluctuations in energy supply via the power-to-gas process that converts excess electricity to H_2 as the reducing agent in CO_2 methanation [78].

Equations (4) and (5) present the Sabatier reaction and reverse water–gas shift (RWGS), corresponding to the hydrogenation of CO_2 to methane and CO, respectively. Thermodynamically, the former reaction dominates at T < 500 °C, while the latter at T > 500 °C. However, as presented in Table 2, the selectivity toward CO and methane is greatly altered on the heterogeneous catalysts with the combination of various metals and supports.

$$CO_2 + 4H_2 \rightarrow CH_4 + 2H_2O \tag{4}$$

$$\Delta H_{298K} = -165 \text{ kJ/mol}$$

$$CO_2 + H_2 \rightarrow CO + H_2O \tag{5}$$

$$\Delta H_{298K} = 41 \text{ kJ/mol}$$

Table 2. Performance of the selected catalysts for CO_2 hydrogenation to CO and CH_4.

Catalyst	T (°C)	P (MPa)	H_2/CO_2/Inert	GHSV (mL g^{-1} h^{-1})	X_{CO2} (%)	S_{CO} (%)	S_{CH4} (%)	Reference
Ru/MnO$_x$					25	10	90	
Ru/Al$_2$O$_3$					32	6	94	
Ru/CeO$_2$	300	0.1	22/5/73	150,000	83	1	99	[78]
Ru/ZnO					1	94	6	
PtCo/TiO$_2$					8.2	99	1	
PtCo/CeO$_2$	300	0.1	67/33/0	36,000	9.1	92	8	[82]
PtCo/ZrO$_2$					7.8	90	11	
Co/ZrO$_2$					92.5	< 1	> 99	
Co/SiO$_2$					80.1	2	98	
Co/Al$_2$O$_3$	400	3.0	80/20/0	3600	77.8	3	97	[81]
Co/TiO$_2$					30.9	96	4	
Ni/ZIF-8 [a]	420	0.1	80/20/0	15,000	43.8	97	3	[81]
Fe/ZIF-8 [a]					43.8	97	3	
Ni/Fe/ZrO$_2$	230	0.5	80/20/0	5000	82	14	86	[83]
γ-Fe$_2$O$_3$	400	0.1	20/0.1/80	1,500,000	45	30	70	[84]
Ni/MCM [b]	400	0.1	80/20/0	90,000	73.2	8	92	[85]

[a] ZIF-8, a zinc-based zeoliticimidazolate framework, is pyrolyzed before metal doping; [b] MCM as zeolite.

In the presence of noble metals, CO_2 hydrogenation to CO can be realized at a low temperature. This phenomenon is attributed to the lower activation energy of the hydrogenation process on the active sites of metals [86]. For instance, Dietz et al. (2015) have simulated RWGS at the (111) plane of several metals and found that Ni, Cu, and Rh favor the dissociation of $CO_2 \rightarrow CO + O$, while Ag, Pd, and Pt prefer the hydrogenation pathway: $CO_2 + H \rightarrow COOH$ [86]. When Pt is loaded on silica and titania, the support itself enhances CO_2 adsorption. The energy change of CO to HCO governs the selectivity toward CO, while the competition for *H_2COH between hydrogenation and C–O bond cleavage affects the preferential production of CH_4 or CH_3OH [87]. The performance of Pt on RWGS is enhanced by the addition of a potassium promoter, which enables the formation of Pt-O(OH)-K interfacial intermediate that promotes the adsorption of the bicarbonate species, the precursor of CO via the formate pathway. CO_2 conversion in the K-promoted Pt/zeolite system at 500 °C is 27.4%, which is 2-fold greater than the system without K-promoters [88]. Kattel et al. (2016) further reported that the interfacial sites between PtCo alloy and other reducible oxides (CeO$_2$, TiO$_2$ and ZrO$_2$) are important to stabilizing surface intermediates [82]. Wang et al. (2015) have studied the mechanisms of

CO_2 hydrogenation over Pd/Al_2O_3 and concluded that RWGS and the Sabatier reaction do not take place at the same surface sites [89].

Ru-based catalysts show great catalytic methanation at a low temperature. Dreyer et al. (2017) have investigated the hydrogenation of CO_2 using Ru-based catalysts dispersed on different metal oxide supports, including Al_2O_3, ZnO, MnO_x, and CeO_2 [78]. They have found that methanation occurs by partial reduction at metal oxides supports, which increases the coverage of H* but strengthens the C–O bond of CO*. The highest CO_2 conversion (83%) and methane selectivity (99%) at 300 °C is obtained by the Ru/CeO_2 system [78]. Guo et al. (2018) have demonstrated the metal-support interactions and the effect of H-spillover on CO_2 methanation [90]. By varying the degree of Ru dispersion from the size of a single atom to nanoparticle (4 nm) on Ru/CeO_2, metal-support interaction is the strongest for a single-atom Ru/CeO_2 that facilitates CO* activation, whereas H-spillover prevails in large Ru clusters and prevents the catalyst from poisoning by enhanced H_2O removal [90]. Thus, controlling the size of Ru at around 1.2 nm achieves an appropriate balance between the two phenomena, leading to a turnover rate of 1.6-fold and 14-fold greater than single-atom and 4-nm Ru, respectively [90]. The interactions between Ru and TiO_2 are fortified by syngas pretreatment at 600 °C, which leads to an increase in interfacial sites on $Ru-TiO_2$ by encapsulation of Ru [91]. Hydrogenation of CO_2 on nickel-based catalysts has been explored extensively. Dispersing Ni on SiO_2 support is deterministic of selectivity, in which the 10 wt% Ni/SiO_2 is effective in stabilizing the monodentate configured HCOO intermediate, which does not occur on catalysts of low Ni loadings (0.5 wt%) [92]. Bi et al. (2019) have demonstrated that impregnating Ni on an MCM zeolite with a sodium-free alkaline agent enhances the synergism between Ni and NiO during CO_2 hydrogenation via H_2 adsorption and CO_2 activation, respectively [85]. The catalyst exhibits remarkable CO_2 conversion (68.3%) and methane selectivity (91.4%) with high stability [85]. Doping Ni/ZrO_2 with iron enhances the reducibility of Ni and ZrO_2 owning to the electron-donating property of Fe(II), which in turn promotes the synergism effects of Ni-NiO and metal-support interactions [83,93].

Based on the above discussions, it is noted that in addition to the reactivity of CO2R catalysts, the chemical environment of the support also plays an important role in CO2R selectivity in the gaseous phase. This is because the gaseous abiotic OC2R is conducted in a high temperature (in comparison with the condition of the aqueous CO2R). In this configuration, the dispersion of CO2R catalysts and consequently their contact with support is highly sensitive to the stability of support. A relative alkaline support such as alumina is beneficial for CO2R efficiency as CO_2 is regarded as a weak acid in this configuration. It is thus suggested that in addition to the characteristics of the CO2R catalyst, its dispersion over the support is another issue of concern for rationally engineering a CO2R catalyst with high selectivity and efficiency.

3.2.2. Hydrogenation of CO_2 to Methanol

Methanol is a valuable CO_2 reduction product as it can be served as biofuel, building blocks in organic synthesis, and fuels for a methanol-based fuel cell. Table 3 shows CO_2 conversion to methanol at a pressure of 1–4 MPa over different metallic meal oxide catalysts. Catalyst $Cu/Zn/Al_2O_3$ plays an important role in the commercial methanol production from syngas. DFT studies reveal that the stabilization of the transition surface species is the key to achieving high selectivity in the syngas conversion. The formate pathway predominates the total process on the surface of $Cu/ZnAl_2O_4$ and $Cu/Zn/Al_2O_3$, in which the rate-limiting step is the formation of H_2COO* and H_2COOH* [94,95]. The CO production via RWGS is the major byproduct in methanol synthesis. Based on the H/D isotope substitution technique, it is known that methanol synthesis and RWGS occurrence take place at difference surface sites on $Cu/ZnO/Al_2O_3$, Cu/MgO, Cu/SiO_2, and Pd/SiO_2 [96]. Karelovic and Ruiz (2015) have suggested that ZnO loads with larger Cu particles tend to suppress the activity of RWGS as the specific methanol formation rate per surface Cu is independent of Cu particle size, while that of CO is enhanced by smaller

Cu particles [97]. Ro et al. (2016) have studied the synergistic effect by dispersing Cu on ZrO_2 and reported that the rate constant of CO_2 conversion on Cu-ZrO_2 interfacial is eight times greater than that on plain Cu [98]. Phongamwong et al. (2017) have added colloidal silica on Cu/Zn/ZrO_2 as geometric spacers to enhance the stability and performance of the Cu-based catalysts in CO_2 hydrogenation [99]. The authors have reported that 1% of SiO_2 loading increases the methanol synthesis activity by 26% and retains 12% more activity after emerging from the steam for 96 h at 280 °C.

Table 3. Performance of the selected catalysts for CO_2 hydrogenation to methanol.

Catalyst	T (°C)	P (MPa)	CO_2/H_2/Inert	GHSV (mL g^{-1} h^{-1})	X_{CO2} (%)	S_{CH3OH} (%)	Reference
Cu/SiO_2	250	4.1	72/24/4	3600	2.8	15	[100]
Cu/ZnO	180	0.7	90/10/0	4000	0.9	94	[97]
Cu/ZnO/ZrO_2/SiO_2	240	2.0	30/90/10	39,000	5.2	38	[99]
Cu/ZnO/ZrO_2/MgO/Al_2O_3	250	2.0	75/25/0	2000	12.1	36	[93]
Pd/ZnO	250	2.0	25/75/0	3600	10.7	60	[101]
Pd/SiO_2	250	4.1	72/24/4	3600	3.0	23	[100]
Pd-Cu/SiO_2					6.6	34	
Pd-Cu/SiO_2	250	5.0	75/25/0	30,000	1.6	27	[102]
MnO_x-Co_3O_4	250	1.0	60/20/20	120,000	45.1	22	[103]
In_2O_3	270	4.0	60/20/20	15,000	1.1	55	[76]
In_2O_3	330	4.0	60/20/20	15,000	7.1	40	
In_2O_3/ZrO_2	300	5.0	80/20/0	16,000	5.2	>99	[104]

Bimetallic Pd, such as PdZn and PdCu, exhibits a high methanol yield similar to Cu-based catalysts even at low temperatures [73]. The Pd dispersed in ZnO shows exceptional stability attributed to the particle size being maintained at 5 nm even after pre-reduction at 400 °C. While the colloidal dispersion technique is effective in stabilizing the interfacial sites of PdZn, its methanol formation yield is 40-fold greater than the same catalysts synthesized by the traditional wet impregnation method [101]. PdCu and $PdCu_3$ bimetallic catalysts exhibit a methanol formation rate of 0.31 μmol gcat^{-1} s^{-1}, which is 3.4-fold and 6.2-fold greater than monometallic Pd and Cu, respectively [100]. Results of DFT simulation further indicates that the (111) plane of PdCu is highly active in methanol evolution, particularly at the low-coordinated Pd on the stepped surface [102]. Furthermore, methanol evolution through the formate pathway again is the major catalytic reaction, which can be further promoted by adsorbing small amounts of water to lower the energy barrier through the H-shuttled mechanism [102]. A novel metal-free In_2O_3 catalyst is also known to exhibit high selectivity in reducing CO_2 to methanol [76]. The oxygen vacancies on In_2O_3 are important to CO_2 hydrogenation. Specifically, the In_2O_3 with optimal oxygen vacancy exhibits a methanol yield of 3.7 mol kg-cat^{-1} h^{-1}, CO_2 conversion of 7.1%, and methanol selectivity of 40%, respectively, at 330 °C and 4 MPa [75]. Martin et al. (2016) have reported that the selectivity toward methanol over In_2O_3 approaches 100% in the temperature range of 200–300 °C [104]. The methanol yield is further promoted by increasing the density of surface oxygen vacancy through Ar sputtering, syngas pretreatment, and ZrO_2 support [104]. Likewise, incorporating a small fraction of Mn into the spinel Co_3O_4 structure greatly enhances the methanol selectivity in CO_2 hydrogenation, likely attributed to the increase in surface basicity [103]. In brief, the significance of the thermal stability of the support in the CO2R to methanol is relatively less profound than that in the CO2R to CO and methane. This is because the former is usually carried out in a relatively lower temperature than that of the latter. In this case, the surface basicity becomes much more significant in affecting the reactivity of CO2R catalysts.

3.2.3. Hydrogenation of CO_2 to Low and Long Chain Chemicals

CO_2 conversion to lower olefins (C_2–C_4), building blocks, and other long chain hydrocarbons in the gasoline range (C_5–C_{11}) or diesel range (C_{12}–C_{21}) has been explored extensively. Again, catalysts that are reactive in both CO_2 hydrogenation and the Fisher–Tropsch reaction will be capable of achieving the CO_2 conversion objectives [105]. Table 4 lists the performance of CO_2 hydrogenation to low and long chain hydrocarbons on Fe-based catalysts. Upon CO_2 hydrogenation to different hydrocarbons, the Fe-based catalysts undergo consecutive phase transitions together with the creation of multivalent charges and this surface reconstruction process further diversifies distinct active sites on the catalyst [84]. The creation of multivalent charges results in the spinel iron (Fe_3O_4) being composed of Fe_3O_4, iron carbides, and α-iron, which enhance the activity of RWGS, carbon chain growth, and olefins' secondary reactions [106]. It is therefore suggested that an appropriate fraction of Fe_3O_4 and Fe_5C_2 is necessary for the production of high olefin and paraffin [107,108]. Pretreatment of Co-Fe bimetallic under various reducing gases (i.e, H_2, syngas, and CO) is another effective ex-situ modification strategy to precisely control the phase transition [77]. Under the selected reducing environment, CO activation leads to the formation of CoFe alloy and carburized phases (Co_2C and FeC_x) that shift the selectivity toward low hydrocarbons and oxygenate [77]. While most Fe-based catalysts produce lower hydrocarbons, delafossite ($CuFeO_2$) exhibits high selectivity toward long chain hydrocarbons (C_5^+) and 85 wt% of the produced long chain hydrocarbons are in the gasoline and diesel range [109]. Doping alkali metals on Fe-based catalysts is also beneficial to chain growth propagation due to stronger CO_x adsorption [106]. Compared to Na-free Fe_3O_4, incorporating 1.18 wt% of Na greatly enhances the CO_2 conversion and selectivity toward light olefin from 29.3 to 40.5% and 0.1 to 40.3%, respectively [110]. The presence of potassium promoter on Fe-Co/Al_2O_3 diminishes the density of hydrogen on metal surfaces, which in turn suppresses the hydrogenation of olefins [111].

Table 4. Performance of the selected catalysts for CO_2 hydrogenation to hydrocarbons.

Catalyst	T (°C)	P (MPa)	H_2/CO_2/Inert	GHSV (mL g^{-1} h^{-1})	X_{CO_2} (%)	S_{CO} (%)	Hydrocarbon Distribution (%)				Reference
							CH_4	$C_2^=$-$C_4^=$	C_2^--C_4^-	C_{5+}	
Fe_3O_4	320	3	72/24/4	2000	29	17	60	<1	36	3	[110]
Na-Fe_3O_4	320	3	72/24/4	2000	41	14	16	47	8	30	
Fe_2O_3	350	1.5	70/23/7	1150	23	21	18		82		[107]
K-Fe_3O_4/Fe_2O_3	270	5	73/25/2	2700	37	14	24	42	9	29	[106]
$CuFeO_2$	300	1	75/25/0	1800	18	32	4	31	5	60	[109]
$CuFe_2O_4$	300	1	75/25/0	1800	16	28	38	1	49	11	
K-Fe-Co/Al_2O_3	300	1.1	72/24/4	700	31	18	16	27	6	51	[111]
Co/Fe oxide [a]	270	0.9	72/28/0	2000	27	14	82		15	<1	[77]
Na-Co/Fe oxide [a]	270	0.9	72/28/0	2000	23	42	60		29	2	
Pyrolyzed Fe-MIL-88B [b]	400	3	75/25/0	3600	46	18	32	23	18	27	[108]
K-pyrolyzed Fe-MIL-88B [b]	400	3	75/25/0	3600	43	26	32	33	6	19	
In_2O_3/HZSM	340	3	73/24/3	9000	13	45	1		20	79	[112]
Ga_2O_3/HZSM	340	3	73/24/3	9000	9	86	5		35	61	
Fe_2O_3/HZSM	340	3	73/24/3	9000	7	74	2		28	71	
Na-Fe_3O_4/HZSM	350	3	72/24/4	4000	33	26	8		18	74	[105]
In_2O_3-ZrO_2/SAPO	400	3	73/24/3	9000	36	85	4	76	17	3	[75]

[a] Pre-carburized under CO stream at 250 °C; [b] Fe-MIL-88B is an iron-based metal organic framework.

Bifunctional catalysts have emerged actively in synthesizing hydrocarbons from CO_2 with great flexibility. Combined In_2O_3 and zeolite (HZSM-5) effectively synthesizes liquid fuels (C_{5+}) from CO_2 by suppressing undesired C_1 products [112]. In the process, CO_2

is first hydrogenated to methanol at the reduced site on In_2O_3. Methanol that diffuses to the acidic site of zeolite transforms to hydrocarbons by the hydrocarbon-pool mechanism, which results in 78.6% of C_{5+} hydrocarbons [112]. Replacing the zeolite HZSM-5 by SAPO-34 increases the selectivity toward lower olefins, probably as a result of changes in topology [74]. Notably, the bifunctional catalyst must be packed in granular instead of powder form as the surface acidity of the zeolite support is another important factor controlling the selectivity of CO_2 hydrogenation toward hydrocarbons [112]. HZSM-5/Na-Fe_3O_4 composite also effectively converts CO_2 to hydrocarbons in the gasoline range [110]. The above catalyst composites provide three distinct active sites: Fe_3O_4 sites for RWGS, Fe_5C_2 sites for FTS, and zeolites for oligomerization [105]. Na-Fe_3O_4/HZSM shows little deactivation; the CO_2 conversion and C_{5+} selectivity remain at 27% and 54%, respectively, over 1000 h of operation [105]. Based on the above discussions, it is noted that the surface chemistry of the support is of equal importance to catalysts in CO2R. Interestingly, surface acidity instead of surface basicity is much more important in this case as the development of long chain chemicals strongly relies on the hydride transfer.

In short, there are advances in the development of heterogeneous catalysts for CO_2 hydrogenation in recent years due to a better understanding of the elementary reactions via DFT simulation, catalytic performance of metal-support, and metal-dopant interfacial sites. With appropriate modifications, CO_2 can be hydrogenated to CO, CH_4, CH_3OH, and other low and long chain hydrocarbons. Further challenges are reducing cost and increasing durability of catalysts, reducing cost of renewable hydrogen sources, and carbon dioxide capture.

4. Biotic CO2R

Biological CO2R has been around for a long period of time. CO2R by microalgae cultivation takes additional advantage over terrestrial plants because the photosynthesis efficiency of the former is about 10~50 times greater than that of the latter system [113]. The additional advantage of microalgae cultivation over other higher plants lies in this capability of being spatially cultivatable. Spatial arrangement can effectively maximize the land usage in accordance with the theme of the UN Sustainable Development Goals in which the balance among the natural science, social science, and stakeholders is particularly emphasized. Research activities, such as screening for appropriate microbial species, developing a novel cultivation strategy, and separating value-add byproducts have attracted much attention. Nutrient removal and recovery from nutrient-rich wastewater is an additional bonus of microalgal CO2R [114]. Sunlight, algal, carbon source, and nutrients are four essential components in microalgae CO2R as shown in Equation (1), which can be operated in open (outdoor with ponds and raceway reactors) or closed systems (indoor with columns) [113,115]. The crucial component in biological CO2R facilities is the photobioreactors (PBRs), which can be assembled in a variety of configurations, such as tubular, flat-plate, bubble column, and airlift PBR. CO_2 bubbles are injected at the bottom of PBR to facilitate gas–liquid transport [116]. Operation variables include gas aeration rate (volumetric gas flow rate per unit volume of culture medium, vvm), biomass productivity (dry cell weight, DCW, per liter of medium per day, (g-DCW L^{-1} d^{-1})), specific growth (d^{-1}), and CO_2 sequestration/fixation rate (g-CO_2 L^{-1} d^{-1}) [117,118].

4.1. Biotic CO2R by Microalgae Farming

Table 5 summarizes the performance of different algal species in biological CO2R. *Chlorella* is a genus of green algae that has been widely studied due to its fast growth rate. In the *Chlorella* family, *Chlorella* sp. and *Chlorella vulgaris* exhibit the highest CO2R rates and highest lipid productivity (precursor of biodiesel) over others [119–121]. *Scenedesmus* sp., a microalga isolated from a marble mining site, is active at a high CO_2 stream (~15% CO_2) [122]. *Asterarcys quadricellulare* and *Chlorella sorokiniana* isolated from water bodies near a steel plant, survive at a high CO_2 concentration (15%) and temperature (40 °C) [123]. Yun et al. (2016) isolated *Acutodesmus obliquus* from an acid mine drainage site that remains

active in an acidic environment [124]. Microalgae collected from a domestic wastewater treatment plant (WWTP) remains active even under 50% CO_2 (without aeration) in pH 7 to pH 11 [125]. In addition to naturally occurring microalgae, genetic engineered *Chlorella* sp. is able to survive in an alkaline environment (pH 6~11) with a biomass productivity 12-fold higher than the wild type [126]. Introducing an aldolase gene of cyanobacteria into the chloroplast of *Chlorella vulgaris* increases the biological CO2R efficiency by 1.2 times that of the original strain [127]. Li et al. (2015) have reported that genetic engineered *Chlorella* sp. is tolerable to high CO_2 concentration and exhibits a biomass yield of 4.06 and 3.68 g-L^{-1} in 1 and 30% CO_2, respectively, which are 1.3-fold and 3-fold that of the original strain [128]. The mixed culture of nitrifying bacteria and *Chlorella* exhibits a synergetic effect that enables biological CO2R at relatively high dissolved oxygen while achieving high biomass production (23%) [129].

In light of the cultivation condition, it is known that factors including pH, light intensity, temperature, level and form of carbon, nitrogen, and phosphate and trace elements significantly affect the efficiency and biomass composition of biological CO2R. The microalgae cultivation is often conducted at neutral pH (*ca.* 7~9). Acidification occurs mainly by dissolution of NO_x and SO_x and to a lesser extent CO_2, and complicates the biological CO2R, especially when flue gas is the sole carbon source. The addition of pH buffers, such as phosphates [130], HEPES [123] and bicarbonate [131] minimizes pH fluctuation. An intermittent gas injection strategy based on pH feedback precisely controls the pH of the growth medium within a 0.5 unit [132]. Vo et al. (2018) have studied the performance of *Chlorella* sp. and reported that the highest CO_2 fixation rate (1.65 g-CO_2 L^{-1} d^{-1}) is an N:P ratio of 15:1 [133]. Domestic wastewater [134,135], aquaculture wastewater [120,136], and landfill leachate [137] can serve as nutrient sources for microalgae cultivation to lower operational costs. Liu et al. (2017) have reported that *Chlorella vulgaris,* cultivated using WWTP effluent discharge, consumes ammonia then nitrate [134]. On the other hand, Fu et al. (2019) have reports that feeding urea to *Chlorella vulgaris* instead of nitrate as a nitrogen source increases the biomass productivity by 14%, and a low dose of D-glucose could stimulate its photoautotrophic biomass production [138].

CO_2 fixation efficiency and biomass productivity are highly related to CO_2 concentration in gas aeration and the injection modes of bioreactors. Posadas et al. (2015) have showed that the metabolic pathway of *Chlorella vulgaris* is sensitive to dissolved inorganic carbon concentrations [135]. Gonçalves et al. (2016) have studied the effect of CO_2 concentration on biological CO2R of algae, i.e., *Chlorella vulgaris* and *Pseudokirchneriella subcapitata*, and cyanobacteria, i.e., *Synechocystissalina* and *Microcystis aeruginosa* and reported that the optimal CO_2 concentration is 5.35 ± 0.34% [118]. Intermittent aeration of 10% CO_2 to mutated *Chlorella* sp. achieves a CO_2 utilization efficiency of 20.4%, which is 5-fold greater than continuous aeration. The rate of CO_2 biosequestration in the continuous mode is greater than that of the injection mode (1.61 vs. 1.33 g d^{-1}) [126]. The rate of biomass production and CO_2 biosequestration are closely proportional to light intensity. However, algal growth at different life stages requires a different spectrum and intensity of light. Dineshkumar et al. (2016) have reported that the light intensity of 50~125 μmol m^{-2} s^{-1} is enough to sustain *Chlorella minutissima* initially (~24 h) [139]. Xie et al. (2014) have demonstrated that increasing light intensity on *Desmodesmus* sp. improves CO_2 biofixation rate [117].

Table 5. Performance of the selected catalysts for CO_2 hydrogenation to hydrocarbons.

Microalgae Species	CO_2 Conc. (v/v%)	CO_2 Fixation Rate (g-CO_2 L^{-1} d^{-1})	Biomass Production Rate (g-DCW L^{-1} d^{-1})	Specific Growth Rate (d^{-1})	Cultivation System	CO_2 Injection Rate (vvm), Mode	Light Intensity (umol m^{-2} s^{-1}), Light/Dark Cycle	Reference
Acutodesmusobliquus	14.1	0.22 [b]	0.12	1.09	Flask	1.66, intermittent	120, 24/0	[124]
Aphanothecemicroscopica Nägeli	15 [a]	14.14 (from carbon balance)	0.47	1.4	Bubble column	1, intermittent	150, 24/0	[140]
Asterarcysquadricellulare	5 [a]	0.39 [b]	0.21	1.2	Flask	0.5, continuous	250, 14/10	[123]
Chlorella minutissima	3.5	1.17	0.64	1.66	Airlift	0.43, continuous	50~260 [f], 24/0	[139]
Chlorella sorokiniana	5 [a]	0.39 [b]	0.22	2.42	Flask	0.5, continuous	250, 14/10	[123]
Chlorella sorokiniana	15.6	0.31	0.17	0.46	Airlift	0.33, continuous	120, 24/0	[121]
Chlorella sp.	1	1.00	0.53	0.615	Flat-panel	0.25, continuous	130, 24/0	[131]
Chlorella sp.	2	0.77 [b]	0.42	0.62	Bubble column	0.2, continuous	400, 24/0	[115]
Chlorella sp.	3	0.46	0.31	NA	Bubble column	-, continuous	115, 24/0	[119]
Chlorella sp.	5	1.65	0.87	0.15	Bubble column	0.5, continuous	56, 24/0	[133]
Chlorella sp.	5	0.10	0.06	0.25	Flask	No aeration	450, 24/0	[141]
Chlorella sp.	8 [a]	2.33	0.84	1.11	Bubble column	0.2, continuous	300, 24/0	[136]
Chlorella sp. [c]	10	1.33	0.73	0.55	Bubble column	0.2, intermittent	300, 24/0	[126]
Chlorella sp.	12.5 [a]	0.97 [b]	0.53	0.827	Bubble column	0.2, continuous	300, 24/0	[142]
Chlorella sp. [d]	30	0.61 [b]	0.33	NA	Bubble column	0.67, continuous	95, 24/0	[128]
Chlorella vulgaris	2.5	3.71	2.06	NA	Bubble column	0.36, continuous	300, 18/6	[138]
Chlorella vulgaris [e]	3	0.31	0.17	NA	Flask	No aeration	40, 12/12	[88]
Chlorella vulgaris	5	1.32 [b]	0.72	NA	Bubble column	0.1, continuous	160, 24/0	[143]
Chlorella vulgaris	5	0.10	0.12	1.36	Flask	0.5, continuous	160, 24/0	[118]
Chlorella vulgaris	10	0.43	0.26	0.46	Tubular	0.5, continuous	100, 12/12	[120]
Chlorella vulgaris	10	0.31 [b]	0.17	1.34 [c]	Flask	-, intermittent	40, 14/10	[134]
Desmodesmus sp.	2.5	1.58	0.88	NA	Tubular	0.2, continuous	300~1000 [f], 24/0	[117]
Microcystisaeruginosa [g]	5	0.11	0.14	1.5	Flask	0.5, continuous	160, 24/0	[118]
Pseudokirchneriellasubcapitata	5	0.09	0.10	0.89	Flask	0.5, continuous	160, 24/0	[118]
Scenedesmusdimorphus	15 [a]	0.89	0.49	NA	Tubular	0.25, intermittent	100, 24/0	[132]
Scenedesmus sp.	15	0.17 [b]	0.09	NA	Flask	No aeration	-, 16/8	[122]
Synechocystissalina [h]	5	0.11	0.14	1.65	Flask	0.5, continuous	160, 24/0	[118]
Tetraselmissuecica,	5	0.11	0.07	0.29	Flask	No aeration	450, 24/0	[141]
Chlorella sp., *Scenedesmus* sp., *Sphaerocystis* sp., *Spirulina* sp.	20	0.27 [b]	0.15	NA	Flask	No aeration	80, 16/8	[125]

[a] Synthetic or real flue gas; [b] Estimated by assuming that 1.83 g of CO_2 is fixed in every gram of microalgal biomass (Cheah et al., 2015) [112]; [c] Chemically mutated strain by N-methyl-N′-nitro-N-nitrosoguanidine; [d] Evolved under 10% CO_2 after 31 adaptive laboratory evolution cycles; [e] Genetically modified strain; [f] Between 0~36 h; [g] Cyanobacteria; [h] Increased linearly.

4.2. The Unit Processes for Biotic CO2R

Common microalgae farming systems includes batch, fed-batch, and semi-continuous cultivation. Although batch cultivation is easy to operate, nutrient depletion and declining light penetrability owing to biomass accumulation gradually loses its efficiency. Fed-batch supplies nutrients periodically to maintain necessary nutrient levels. For example, Xie et al. (2014) have reported that nitrate concentration at 2 mM is necessary to maximize the productivity of lutein by *Desmodesmus* sp. in the batch reactor [117]. Semi-continuous cultivation, which replaces certain amount of microalgal suspension with fresh medium in order to replenish nutrients and reduce the concentration of biomass, is probably the most common strategy in large-scale algae cultivation [126,144]. Furthermore, Huang et al. (2016) have studied a pre-harvesting cultivation strategy, using filtration to decrease the concentration of microalgal cells, and reported that nitrogen utilization efficiency can reach 76%, which is 1.7-fold that of semi-continuous cultivation [143].

Biological CO2R using flue gas is a highly desirable approach as it directly reduces the CO_2 emission to the atmosphere. In general, flue gas contains 5~15% CO_2 in addition to certain amounts of NO_x, SO_x, and H_2S, which is somewhat harsh to algal growth. A mixed microalgal community collected from a freshwater lake can survive in 100% flue gas (11.2% CO_2, 206 ppm NO_2, and 273 ppm SO_2) [130]. Cultivating *Scenedesmus dimorphus* with synthetic flue gas containing 15% CO_2, 400 ppm SO_2, and 300 ppm NO under continuous aeration can suffer a sudden pH drop that eventually suppresses algal growth. Under such a circumstance, there is the intermittent sparge of flue gas damping pH fluctuation that gives rise to a high productivity of algal biomass and CO_2 removal [132]. The presence of NO_x in the aeration gas is beneficial for microalgae in lipid productivity [123]. Sulphate accumulation up to 870 ppm resulting from the medium recycle has limited influence on CO2R by *Tetraselmi ssuecica*; however, the presence of H_2S inhibits the growth of *Chlorella sorokiniana* [121,144]. In contrast, flue gas from a nature-gas boiler containing 8% CO_2 and being purged continuously at 0.05 vvm exhibits limited influence on *Chlorella* sp. growth [136]. Kuo et al. (2016) have reported that algal biomass production in CO_2 biofixation using *Chlorella* sp. in large-scale bubble column PBRs is the same as that of indoor laboratory scale reactor using flue gas streams that contain 24~26%, 10~80 ppm, and 15~90 ppm of CO_2, NO_x, and SO_2, respectively [136].

4.3. Additional Ecomomic Benefit of Biotic CO2R

The economic benefits of microalgae CO2R are unsettling. Ou-Yang et al. (2018) have argued that carbon sequestration by microalgae is not profitable for coal-fired power plants even with government subsidies and the consideration of carbon price [145]. Zhu et al. (2016) have evaluated the economy of *Chlorella zofingiensis* cultivation in southern China and reported that growing algae with nutrient-rich wastewater significantly reduces the cost of biomass by \$451 tonne^{-1} from savings of water and nutrients, when the credit of wastewater treatment at \$0.55 m^{-3} is counted [146]. The production of one kg of biomass and one L of algal oil cost approximately \$1.2 kg^{-1} and \$3.9 L^{-1}, respectively. Large-scale microalgae cultivation for biofixation of CO_2 is capital intensive and requires massive land space [147]. Therefore, the cost of the microalgae growth facility has tremendous impacts on the economy of CO_2 biofixation. At a photosynthetic efficiency of 4% and target CO_2 fixation of 40%, the make-even market price of microalgae is at least \$440 tonne^{-1}. Therefore, maximizing the revenue of microalgae is vital for biofixation technology from an economic perspective. There are attempts to assess the microalgae economics in terms of algae farming toward energy production, e.g., the unit area of algal biomass production and CO_2 fixation. As shown in Table 5, among a total of 29 references reviewed, the biomass production rate varies by 3 orders of magnitude (0.07–2.06 g-DCW L^{-1} d^{-1}), whereas some specific growth rate (d^{-1}) data are unavailable. Without definitively and reliably consistent data, it is beyond a reasonable challenge to examine the economic feasibility of algal farming. Apart from the economic feasibility assessment, it is certain that for those

existing microalgae farming pilot plants, optimization of the unit process is a top priority as it makes the microalgae farming one step closer to the market-driven business.

4.4. The Utilization of Microalgae Biomass

The conversion of microalgae biomass to valuable products, i.e., biorefinery, is key to overcoming the economical obstacle toward CO_2-derived bioeconomy [148]. Figure 5 depicts the concept of biotic CO2R coupled with further refinery of microalgal biomass to a variety of products, such as biofuel, pigments, health supplements, and pharmaceuticals [149]. As mentioned above, a market-driven CO2R business will definitely be more sustainable. Based on this consideration, CO2R with flue CO_2 will have a strong incentive within the industry as it eventually reduces the carbon footprint in response to the Paris Climate Agreement. Micronutrient reclamation in microalgae farming further allows the biotic CO2R to be integrated with the wastewater treatment system of the agriculture sector [150]. The interest in microalgae biomass as a renewable and sustainable feedstock for biofuels (biohydrogen, biomethane, biodiesel) and various bioproducts has inspired a new focus in biorefinery [151]. Biofuel, pigments, health supplements, and pharmaceuticals derived from the biomass harvest not only give additional economic incentives but also allows for value-added green chemicals.
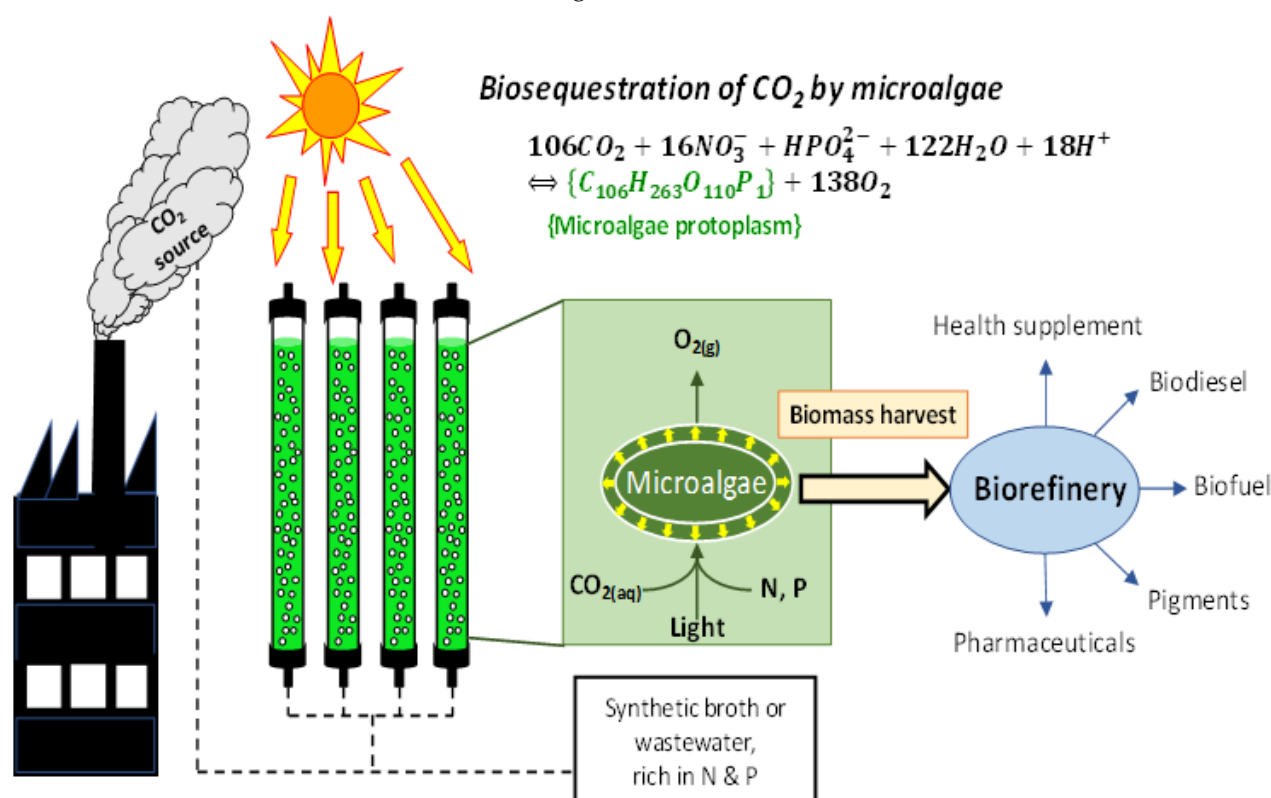
Figure 5. Biosequestration of CO_2 by microalgae and further bio-refinery to valuable products.

Khan et al. (2018) have reported that employing microalgae to convert atmospheric CO_2 to useful products such as carbohydrates, lipids, and other valuable bioproducts through photosynthesis, essentially achieves environmental and economic sustainability [152]. Algae also need N and P as nutrients, which account for 10–20% of algae biomass [153]. These nutrients can be applied as biofertilizer and redeployed in agricultural lands, and the reduction of greenhouse gas (GHG) emissions, which enables meeting the current challenges toward a circular bioeconomy. To meet the increasing food demands, microalgae are potential alternatives to animal and aquatic feeds (i.e., millet, grams, and small fishes) because of the possibility for rapid and eco-friendly cultivation, higher protein content, omega 3 fatty acids, and carotenoids [154,155].

In addition to direct food consumption, microalgae can be feedstock for further conversion to various chemicals and fuels through thermochemical processes, such as liquefication, gasification, and pyrolysis. Liquefication of microalgae takes place in sub/supercritical water, which omits the energy-intensive drying process. The yield and selectivity during thermochemical liquefaction depend on the chemical composition of biomass. The application of sodium carbonate as the homogeneous catalyst promotes a bio-oil yield of carbohydrate-rich microalgae at higher temperatures (300~350 °C) and a bio-oil yield of protein-rich microalgae at low temperatures (250 °C) [156]. Gai et al. (2015) have detailed the reaction pathways of hydrocarbons, proteins, and lipids during hydrothermal liquefaction of *Chlorella pyrenoidosa* and *Spirulina platensis* [157]. Liquefying microalgae over Co/CNTs catalysts improves the biomass conversion and bio-oil yield and enhances the selectivity toward hydrocarbons [158]. On the other hand, the liquid phase produced in hydrothermal liquefaction is rich in phenolic compounds with high nitrogen content [157], which can be further applied to cultivate *Chlorella vulgaris* and *Nannochloropsis gaditana* [159].

Gasification converts carbonaceous substances in microalgae to combustible gases, such as syngas and methane. Conventional gasification, which partially oxidizes dry microalgae under 800~1000 °C and 1~10 bar, is a mature technology but suffers from low thermal efficiency [160]. Raheem et al. (2017) have explored the feasibility of microalgae gasification using air as a gasifying agent and reported that hydrogen gas content is decreased from 24.2 to 19.5% when the loading of biomass is increased from 1 to 2 g in the quartz reactor at the optimal temperature of 95 °C [161]. Supercritical water gasification (SCWG) enables oxidization of wet microalgal biomass in a short reaction time, in which the proper catalyst is crucial for high gas conversion and selectivity toward combustible gases [162]. A continuous SCWG of *Chlorella vulgaris* has been demonstrated in Switzerland to produce methane-rich gas (55~60%) [163].

Chemical looping gasification (CLG) of microalgae is a novel technology that oxidizes biomass to syngas using an oxygen carrier (Me_xO_y, preferably iron ores) in the fuel reactor, while the reduced oxygen carrier (Me_xO_{y-1}) is regenerated in the air reactor [164]. The performance of CLG on *Chlorella vulgaris* is enhanced by microwave pretreatment of biomass and by the adding of CaO to absorb produced CO_2 in the fuel reactor [165,166]. Pyrolysis of microalgal biomass in an oxygen-free environment produces syngas, bio-oil, and char. According to the heating rate and vapor residence time, pyrolysis can be categorized into slow mode (5~10°C min^{-1}, 10~30 s) and fast mode (10~600 °C/min^{-1}, 1~3 s) [160,166]. Wang et al. (2017) have proposed the pyrolysis pathways of carbohydrate, lipid, and protein extraction from *Nannochloropsis* sp [167]. To improve the biofuel and vapor quality produced from pyrolysis, catalytic pyrolysis using zeolite has received much attention. Catalytic cracking of the pyrolysis vapor over zeolite HZSM5 promotes the selectivity toward monocyclic aromatic hydrocarbons, which are important chemical building blocks [168]. Catalytic pyrolysis of *Chlorella vulgaris* on Ni-supported zeolite enhances the quality of bio-oil, which produces less oxygenated and acid compounds compared to non-catalytic pyrolysis [169]. Based on the above discussions, an effective catalyst straightforwardly governs the gasification efficiency. This, once again, signifies the blurry line between the abiotic and biotic CO2R. Knowledge on the rational design of efficient abiotic CO2R catalysts is essential to engineering the surface chemistry of gasification catalysts.

The biological conversion of the harvested microalgal biomass via microorganism includes anaerobic digestion (AD) and fermentation. Anaerobic digestion of the biomass produces biogas containing carbon dioxide and methane through four stages: hydrolysis, acidogenesis, acetogenesis, and ethanogenesis [170]. Fermentation converts microalgal biomass to bio-ethanol in the presence of yeast or bacteria, and to biobutanol through the classic acetone-butanol-ethanol fermentation (ABE) process [171,172]. For both cases, it is necessary to rupture microalgal cells and pretreat biomass to improve the bioavailability, anaerobic biodegradability, and fermentability. The common pretreatments are mechanical, (thermo)chemical, and biological methods. Passos et al. (2015) have reported that

thermal, hydrothermal, and microwave pretreatment of microalgal biomass enhances the bio-methane yield in AD by 72, 28, and 21%, respectively, whereas those by ultrasonication exhibit no significant increase [173]. Alkali thermochemical pretreatment on microalgae with polysaccharide-based cells, e.g., *Chlorella* and *Nannochloropsis*, effectively improves the biomass biodegradability and methane production in AD mode [174]. The enzymatic pretreatment is another effective route to degrade the cell wall and solubilize cellular biomass. Passos et al. (2016) have suggested that the composition of microalgal cell walls (cellulose, hemicellulose, pectin, and glycoprotein) is a critical issue in enzymes selection to achieve maximal biomass solubilization [175]. As for fermentation, the conversion of microalgal carbohydrates to fermentable sugar is accomplished during the pretreatment process. The combination of sulfuric acid treatment and enzymatic hydrolysis achieves maximal sugar release from *Chlorella sorokiniana* and *Nannochloropsis gaditana* (128 mg/g-DCW), while sole sulfuric acid treatment is the most effective method for *Scenedesmus almeriensis* (88 mg/g-DCW) [176]. Shokrkar et al. (2017) have reported that the combination of three thermostable enzymes achieves effective carbohydrates hydrolysis using wet biomass, which lowers the cost by 30% by avoiding drying [177]. When using microalgae as feedstock in the ABE process, sequential alkali-acid pretreatment of *Chlorella vulgaris* removes the proteineous substance in biomass, an inhibitor of ABE fermentation bacteria that increases biobutanol yield [171]. Cheng et al. (2017) have showed that hydrolysis and fermentation can be performed simultaneously in a single reactor to lower the total capital cost and minimize contamination risk [178].

The lipid content in microalgal biomass can be extracted and converted to fatty acid methyl esters (FAMEs), major constituents of biodiesel, by an esterification reaction using an acid/base catalysis within supercritical fluid [149,179]. Lipid extraction, which consumes 90% of overall energy, is the bottleneck toward commercialization of microalgal biodiesel. Recent research focuses on developing green solvent and a novel extraction process to minimize the usage of a conventional chloroform-based solvent, which is costly, flammable, and toxic [180]. Pretreating wet/dry microalgal biomass with surfactants effectively ruptures the cell of microalgae, which enables efficient extraction of lipids using a chloroform-free hexane/isopropanol solvent [181]. Orr et al. (2016) have screened over 30 varieties of room-temperature ionic liquids for microalgal biomass rupture, followed by hexane extraction [182]. Among them, $[C_2mim][EtSO_4]$ gives satisfactory oil recovery of 30 wt% and can be operated with wet microalgal biomass with no deterioration after 5 cycles [182]. The protein and carbohydrate contents in biomass residues after bio-diesel production are richer, which is advantageous to the performance of thermochemical and biological biofuel production [183]. El-Dalatony et al. (2019) have proposed that sequential fermentation of microalgal biomass to bio-ethanol and higher alcohols, followed by biodiesel production from fermentation residue can utilize 89% of biomass [184]. Other than biofuels, valuable biochemicals, such as lutein and C-phycocyanin, can be extracted from microalgae as well [185,186]. To make the process economically feasible, the microalgae farming for CO_2 sequestration must be optimized with respect to the fixation rate of CO_2, the productivity of valuable biochemical compounds, and the biorefinery process of biomass to biofuels.

4.5. The Circular Bioeconomy

Last but not the least; the awareness of the circular bioeconomy has become an irreplaceable consideration in biotic CO2R. The ultimate goal of the circular bioeconomy is to keep the value of products, materials, and resources as long as possible while minimizing waste generation [187]. As discussed above, the operation of separation and thermal units of biorefinery is energy intensive, which means that achieving a neutral carbon footprint while extracting chemicals via biotic CO2R at the same time remains a technical challenge today. In other words, producing value-added chemicals in biotic CO2R to be economically competitive is equally important to reducing atmospheric CO_2 concentration. A recent strengths, weaknesses, opportunities, and threats (SWOT) analysis of organic waste man-

agement based on the circular bioeconomy points out that the logistic cost and supply chain management, seasonality, availability of homogenized organic residue, quality and efficiency of the alternative product, and lack of technical standards and regulation are the main threats and weaknesses [188]. The weakness in the availability of homogenized organic residue is particularly true when extracting high-value chemicals such as hydrocarbons and polysaccharides from algae residues. In this case, advances in fermentation technology will be the solution as it narrows the list of fermentation products [189].

Edging conversion technologies that are capable of efficiently destructing the cell walls of algae such as thermocatalytic processes, mechanochemical depolymerization, and their combination will further facilitate the recovery of high-value chemicals [190]. High-energy efficiency of edging conversion technologies will be the additional bonus that further reduces the carbon footprint in biotic CO2R. Of equal importance is the customized biorefinery procedure through optimizing an algal farming strategy and integrating harvest, extraction, fractionation, and purification processes based on the algae cultivation conditions [191]. The above engineering and technology considerations are essential to reaching the goal of value-added products, materials, and the maintenance of resources in the economy toward circular bioeconomy [192]. Apart from individual technology, integrated approaches of microalgae are promising too. For example, integration of microalgae cultivation with seaweed's anaerobic digestion allows the acquisition of additional biogas. In this case, the methane yield is noted to vary widely depending on the species of microalgae/seaweed and digestion conditions [193]. In-situ transesterification of *Chlorella pyrenoidosa* with spent coffee grounds enhances a 79.9% higher biodiesel yield and better quality of biodiesel than without spent coffee grounds [194]. The application of waste glycerol, which is the byproduct of biodiesel production from scum-derived oil, is also proposed to balance the C/N ratio of the wastewater in microalgae cultivation [195]. Similarly, the addition of lipid-free algal biomass and waste glycerol in the growth medium for microalgae *Scenedesmus obliquus* cultivation increases biodiesel production by ~15% [196]. The above integrated approaches will definitely promote the commercialization of market-driven microalgae-derived biofuel production.

In addition to engineering and technology considerations, job creation and new investment opportunities as the result of the development of a new business model is the unique strength of biotic CO2R [188]. For example, based on the circular bioeconomy concept, algae-based feed supplements and recombinant therapeutic production exhibit the potential in response to increasing aquacultural fish demands worldwide [197]. This is because the algal biomass is rich in protein and lipids that offer enormous opportunities to improve animal health, disease resistance, and yields. In fact, being another important sector of the circular bioeconomy, sustainable aquaculture also seeks a condition to reduce waste production while maintaining the value of products, materials, and resources. In this case, algae can be regarded as a valuable source of key nutrients for high quality fish feeds. Recycling algal residues to produce valuable organic matter for further application in fertilizers or amendments is also possible [198]. This means that the nutrients recovered from algae can be returned to nature to further fertilize the stock feed for livestock. Similarly, manures produced by livestock can be utilized for algae farming [199]. As shown in Figure 6, biotic CO2R plays a contributory role to economic and environmental sustainability and is an indispensable link of the circular bioeconomy.
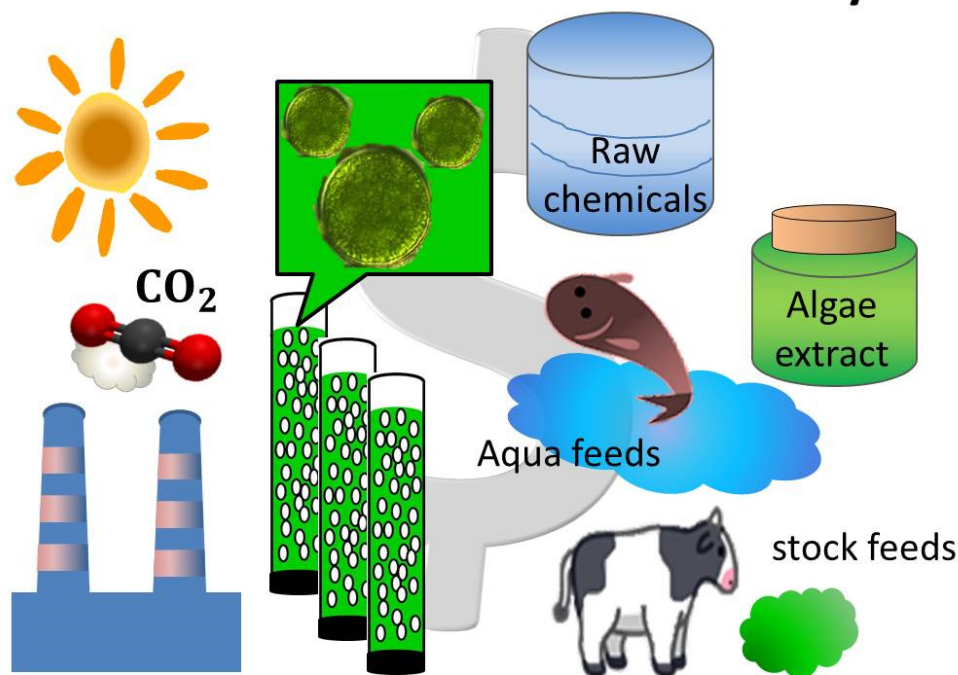
Biotic CO2R for circular bioeconomy

Figure 6. Conceptual presentation on the role of biotic CO2R in the circular bioeconomy.

5. Conclusions

The reduction of atmospheric CO_2 (CO2R) can be achieved through the abiotic or biotic route. Knowledge of the rational design of efficient abiotic CO2R catalysts and optimization of the biotic CO2R unit process straightforwardly govern the success of CO2R. Advances in catalyst engineering enable delicate control of the surface chemistry of catalysts for adsorption/absorption of CO_2/carbonate, surface activation of hydrogen, and stabilization of key intermediates. These surface phenomena not only regulate the abiotic CO2R efficiency but also the selectivity. The latter is another important issue of concern as separation and purification processes require input of external energy. In general, the electrochemical conversion of carbonate in the aqueous phase gives rise to the selective formation of formic acid, while CO_2 hydrogenation in the gaseous phase results in the production of CO, CH_4, methanol, and hydrocarbons. Further technology breakthroughs are needed to design durable and affordable (electrochemical) catalysts with exceptional CO_2 conversion efficiency and selectivity. Promoting biotic CO2R efficiency strongly relies on the resilient microalgae strain and cultivation strategy. The economic feasibility of biotic CO2R remains challenging and additional revenue from microalgae biomass ought to be further maximized through biorefinery by optimizing the cultivation strategy. The latter would be the foundation for the successful implementation of a circular bioeconomy. In addition to the scientific and technological challenges, transdisciplinary cooperation such as the engagement of stakeholders would allow CO2R to be more sustainable.

Institutional Review Board Statement: Not applicable.

Informed Consent Statement: Not applicable.

Data Availability Statement: Not applicable.

Conflicts of Interest: The authors declare no conflict of interest.

References

1. Redfield, A.C.; Ketchum, B.K.; Richards, F.A. The influence of organisms on the composition of sea-water. In *The Sea*; Wiley: New York, NY, USA, 1963; Volume 2, pp. 26–77.
2. Francke, R.; Schille, B.; Roemelt, M. Homogeneously catalyzed electroreduction of carbon dioxide—Methods, mechanisms, and catalysts. *Chem. Rev.* **2018**, *118*, 4631–4701. [CrossRef] [PubMed]
3. Qiao, J.; Liu, Y.; Hong, F.; Zhang, J. A review of catalysts for the electroreduction of carbon dioxide to produce low-carbon fuels. *Chem. Soc. Rev.* **2014**, *43*, 631–675. [CrossRef] [PubMed]
4. Rakowski Dubois, M.; Dubois, D.L. Development of molecular electrocatalysts for CO_2 reduction and H_2 production/oxidation. *Acc. Chem. Res.* **2009**, *42*, 1974–1982. [CrossRef] [PubMed]
5. Mellmann, D.; Sponholz, P.; Junge, H.; Beller, M. Formic acid as a hydrogen storage material—Development of homogeneous catalysts for selective hydrogen release. *Chem. Soc. Rev.* **2016**, *45*, 3954–3988. [CrossRef]
6. Sordakis, K.; Tang, C.; Vogt, L.K.; Junge, H.; Dyson, P.J.; Beller, M.; Laurenczy, G. Homogeneous catalysis for sustainable hydrogen storage in formic acid and alcohols. *Chem. Rev.* **2018**, *118*, 372–433. [CrossRef] [PubMed]
7. Huang, J.Z.; Wang, L.S. Bifunctional wood for electrocatalytic CO_2 reduction to formate and electroanalytical detection of myricetin and cadmium (II). *Electrochim. Acta* **2019**, *319*, 569–576. [CrossRef]
8. Kim, Y.E.; Lee, W.; Youn, M.H.; Jeong, S.K.; Kim, H.J.; Park, J.C.; Park, K.T. Leaching-resistant SnO_2/gamma-Al_2O_3 nanocatalyst for stable electrochemical CO_2 reduction into formate. *J. Indust. Eng. Chem.* **2019**, *78*, 73–78. [CrossRef]
9. Asset, T.; Garcia, S.T.; Herrera, S.; Andersen, N.; Chen, Y.C.; Peterson, E.J.; Matanovic, I.; Artyushkova, K.; Lee, J.; Minteer, S.D.; et al. Investigating the nature of the active sites for the CO_2 reduction reaction on carbon-based electrocatalysts. *ACS Catal.* **2019**, *9*, 7668–7678. [CrossRef]
10. Zhang, N.; Gao, C.; Xiong, Y.J. Defect engineering: A versatile tool for tuning the activation of key molecules in photocatalytic reactions. *J. Energy Chem.* **2019**, *37*, 43–57. [CrossRef]
11. Zhou, L.Q.; Ling, C.; Zhou, H.; Wang, X.; Liao, J.; Reddy, G.K.; Deng, L.Z.; Peck, T.C.; Zhang, R.G.; Whittingham, M.S.; et al. A high-performance oxygen evolution catalyst in neutral-pH for sunlight-driven CO_2 reduction. *Nat. Comm.* **2019**, *10*, 4081. [CrossRef]
12. Yang, D.R.; Yu, H.D.; He, T.; Zuo, S.W.; Liu, X.Z.; Yang, H.Z.; Ni, B.; Li, H.Y.; Gu, L.; Wang, D. Visible-light-switched electron transfer over single porphyrin-metal atom center for highly selective electroreduction of carbon dioxide. *Nat. Comm.* **2019**, *10*, 3844. [CrossRef]
13. Chang, X.X.; Wang, T.; Zhang, P.; Wei, Y.J.; Zhao, J.B.; Gong, J.L. Stable aqueous photoelectrochemical CO_2 reduction by a Cu_2O dark cathode with improved selectivity for carbonaceous products. *Angew. Chim. Int. Ed.* **2016**, *55*, 8840–8845. [CrossRef]
14. Cheng, J.; Zhang, M.; Liu, J.Z.; Zhou, J.H.; Cen, K.F. A Cu foam cathode used as a Pt-RGO catalyst matrix to improve CO_2 reduction in a photoelectrocatalytic cell with a TiO_2 photoanode. *J. Mater. Chem. A* **2015**, *3*, 12947–12957. [CrossRef]
15. Pletcher, D. The cathodic reduction of carbon dioxide—What can it realistically achieve? A mini review. *Electrochem. Comm.* **2015**, *61*, 97–101. [CrossRef]
16. Honoré, M.N.; Belmonte-Ureña, L.J.; Navarro-Velasco, A.; Camacho-Ferre, F. Profit analysis of papaya crops under greenhouses as an alternative to traditional intensive horticulture in southeast Spain. *Int. J. Environ. Res. Public Health* **2019**, *16*, 2908. [CrossRef]
17. Hamnett, A. Mechanism and electrocatalysis in the direct methanol fuel cell. *Catal. Today* **1997**, *38*, 445–457. [CrossRef]
18. Liu, H.; Song, C.; Zhang, L.; Zhang, J.; Wang, H.; Wilkinson, D.P. A review of anode catalysis in the direct methanol fuel cell. *J. Power Sources* **2006**, *155*, 95–110. [CrossRef]
19. Jiang, J.; Wieckowski, A. Prospective direct formate fuel cell. *Electrochem. Comm.* **2012**, *18*, 41–43. [CrossRef]
20. Bartrom, A.M.; Haan, J.L. The direct formate fuel cell with an alkaline anion exchange membrane. *J. Power Sources* **2012**, *214*, 68–74. [CrossRef]
21. An, L.; Chen, R. Direct formate fuel cells: A review. *J. Power Sources* **2016**, *320*, 127–139. [CrossRef]
22. Aresta, M. *Carbon Dioxide as Chemical Feedstock*; Wiley-VCH: Weinheim, Germany, 2010.
23. Brennführer, A.; Neumann, H.; Beller, M. Palladium-catalyzed carbonylation reactions of aryl halides and related compounds. *Angew. Chem. Int. Ed.* **2009**, *48*, 4114–4133. [CrossRef] [PubMed]

24. Liu, Q.; Zhang, H.; Lei, A. Oxidative carbonylation reactions: Organometallic compounds (R-M) or hydrocarbons (R-H) as nucleophiles. *Angew. Chem. Int. Ed.* **2011**, *50*, 10788–10799. [CrossRef]

25. Pegis, M.L.; Roberts, J.A.S.; Wasylenko, D.J.; Mader, E.A.; Appel, A.M.; Mayer, J.M. Standard reduction potentials for oxygen and carbon dioxide couples in acetonitrile and N,N-dimethylformamide. *Inorg. Chem.* **2015**, *54*, 11883–11888. [CrossRef] [PubMed]

26. Gai, S.L.; Yu, J.L.; Yu, H.; Eagle, J.; Zhao, H.; Lucas, J.; Doroodchi, E.; Moghtaderi, B. Process simulation of a near-zero-carbon-emission power plant using CO_2 as the renewable energy storage medium. *Int. J. Greenh. Gas Control* **2016**, *447*, 240–249. [CrossRef]

27. Sun, Z.; Zeng, L.; Russell, C.K.; Assabumrungrat, S.; Chen, S.Y.; Duan, L.B.; Xiang, W.G.; Gong, J.L. Solar–wind–bio ecosystem for biomass cascade utilization with multigeneration of formic acid, hydrogen, and graphene. *ACS Sustain. Chem. Eng.* **2019**, *7*, 22558–22568. [CrossRef]

28. Zouaoui, N.; Ossonon, B.D.; Fan, M.Y.; Mayilukila, D.; Garbarino, S.; de Silveira, G.; Botton, G.A.; Guay, D.; Tavares, A.C. Electroreduction of CO_2 to formate on amine modified Pb electrodes. *J. Mater. Chem. A* **2019**, *7*, 11272–11281. [CrossRef]

29. Benson, E.E.; Kubiak, C.P.; Sathrum, A.J.; Smieja, J.M. Electrocatalytic and homogeneous approaches to conversion of CO_2 to liquid fuels. *Chem. Soc. Rev.* **2009**, *38*, 89–99. [CrossRef]

30. Xu, S.Z.; Carter, E.A. Theoretical insights into heterogeneous (photo)electrochemical CO_2 reduction. *Chem. Rev.* **2019**, *119*, 6631–6669. [CrossRef]

31. Nitopi, S.; Bertheussen, E.; Scott, S.B.; Liu, X.Y.; Engstfeld, A.K.; Horch, S.; Seger, B.; Stephens, I.E.L.; Chan, K.; Hahn, C.; et al. Progress and perspectives of electrochemical CO_2 reduction on copper in aqueous electrolyte. *Chem. Rev.* **2019**, *119*, 7610–7672. [CrossRef]

32. Ma, M.; Trzesniewski, B.J.; Xie, J.; Smith, W.A. Selective and efficient reduction of carbon dioxide to carbon monoxide on oxide-derived nanostructured silver electrocatalysts. *Angew. Chem. Int. Ed.* **2016**, *55*, 9748–9752. [CrossRef]

33. Taheri, A.; Thompson, E.J.; Fettinger, J.C.; Berben, L.A. An iron electrocatalyst for selective reduction of CO_2 to formate in water: Including thermochemical insights. *ACS Catal.* **2015**, *5*, 7140–7151. [CrossRef]

34. Rosas-Hernández, A.; Junge, H.; Beller, M.; Roemelt, M.; Francke, R. Cyclopentadienone iron complexes as efficient and selective catalysts for the electroreduction of CO_2 to CO. *Catal. Sci. Technol.* **2017**, *7*, 459–465. [CrossRef]

35. Buckley, A.K.; Lee, M.; Cheng, T.; Kazantsev, R.V.; Larson, D.M.; Goddard, W.A., III; Toste, F.D.; Toma, F.M. Electrocatalysis at organic-metal interfaces: Identification of structure-reactivity relationships for CO_2 reduction at modified Cu surfaces. *J. Am. Chem. Soc.* **2019**, *141*, 7355–7364. [CrossRef]

36. Lobaccaro, P.; Singh, M.R.; Clark, E.L.; Kwon, Y.; Bell, A.T.; Ager, J.W. Effects of temperature and gas-liquid mass transfer on the operation of small electrochemical cells for the quantitative evaluation of CO_2 reduction electrocatalysts. *Phys. Chem. Chem. Phys.* **2016**, *18*, 26777–26785. [CrossRef] [PubMed]

37. Tomisaki, M.; Kasahara, S.; Natsui, K.; Ikemiya, N.; Einaga, Y. Switchable product selectivity in the electrochemical reduction of carbon dioxide using boron-doped diamond electrodes. *J. Am. Chem. Soc.* **2019**, *141*, 7414–7420. [CrossRef] [PubMed]

38. Hori, Y. *Modern Aspects of Electrochemistry*; Vayenas, C.G., White, R.E., Gamboa-Aldeco, M.E., Eds.; Springer: New York, NY, USA, 2008.

39. Taheri, A.; Berben, L.A. Tailoring electrocatalysts for selective CO_2 or H^+ reduction: Iron carbonyl clusters as a case study. *Inorg. Chem.* **2016**, *55*, 378–385. [CrossRef] [PubMed]

40. Waldie, K.M.; Ostericher, A.L.; Reineke, M.H.; Sasayama, A.F.; Kubiak, C.P. Hydricity of transition-metal hydrides: Thermodynamic considerations for CO_2 reduction. *ACS Catal.* **2018**, *8*, 1313–1324. [CrossRef]

41. Kortlever, R.; Shen, J.; Schouten, K.J.P.; Calle-Vallejo, F.; Koper, M.T.M. Catalysts and reaction pathways for the electrochemical reduction of carbon dioxide. *J. Phys. Chem. Lett.* **2015**, *6*, 4073–4082. [CrossRef]

42. Yu, X.; Pickup, P.G. Recent advances in direct formic acid fuel cells (DFAFC). *J. Power Sources* **2008**, *182*, 124–132. [CrossRef]

43. Feaster, J.T.; Shi, C.; Cave, E.R.; Hatsukade, T.; Abram, D.N.; Kuhl, K.P.; Hahn, C.; Nørskov, J.K.; Jaramillo, T.F. Understanding selectivity for the electrochemical reduction of carbon dioxide to formic acid and carbon monoxide on metal electrodes. *ACS Catal.* **2017**, *7*, 4822–4827. [CrossRef]

44. Shinagawa, T.; Larrazábal, G.O.; Martín, A.J.; Krumeich, F.; Pérez-Ramírez, J. Sulfur-modified copper catalysts for the electrochemical reduction of carbon dioxide to formate. *ACS Catal.* **2018**, *8*, 837–844. [CrossRef]

45. Huan, T.N.; Simon, P.; Rousse, G.; Génois, I.; Artero, V.; Fontecave, M. Porous dendritic copper: An electrocatalyst for highly selective CO_2 reduction to formate in water/ionic liquid electrolyte. *Chem. Sci.* **2017**, *8*, 742–747. [CrossRef]

46. Li, C.W.; Ciston, J.; Kanan, M.W. Electroreduction of carbon monoxide to liquid fuel on oxide-derived nanocrystalline copper. *Nature* **2014**, *508*, 504–507. [CrossRef] [PubMed]

47. Kuhl, K.P.; Cave, E.R.; Abram, D.N.; Jaramillo, T.F. New insights into the electrochemical reduction of carbon dioxide on metallic copper surfaces. *Energy Environ. Sci.* **2012**, *5*, 7050–7059. [CrossRef]

48. Hori, Y.; Murata, A.; Takahashi, R. Formation of hydrocarbons in the electrochemical reduction of carbon dioxide at a copper electrode in aqueous solution. *J. Chem. Soc. Faraday Trans.* **1989**, *1*, 2309–2326. [CrossRef]

49. Hori, Y.; Takahashi, R.; Yoshinami, Y.; Murata, A. Electrochemical reduction of CO at a copper electrode. *J. Phys. Chem. B* **1997**, *101*, 7075–7081. [CrossRef]

50. Hori, Y.; Murata, A.; Takahashi, R.; Suzuki, S. Electroreduction of CO to CH_4 and C_2H_4 at a copper electrode in aqueous solutions at ambient temperature and pressure. *J. Am. Chem. Soc.* **1987**, *109*, 5022–5023. [CrossRef]

51. Li, C.W.; Kanan, M.W. CO_2 reduction at low overpotential on Cu electrodes resulting from the reduction of thick Cu_2O films. *J. Am. Chem. Soc.* **2012**, *134*, 7231–7234. [CrossRef] [PubMed]

52. Gong, M.; Cao, Z.; Liu, W.; Nichols, E.M.; Smith, P.T.; Derrick, J.S.; Liu, Y.S.; Liu, J.; Wen, X.; Chang, C.J. Supramolecular porphyrin cages assembled at molecular–materials interfaces for electrocatalytic co reduction. *ACS Cent. Sci.* **2017**, *3*, 1032–1040. [CrossRef]

53. Bertheussen, E.; Verdaguer-Casadevall, A.; Ravasio, D.; Montoya, J.H.; Trimarco, D.B.; Roy, C.; Meier, S.; Wendland, J.; Nørskov, J.K.; Stephens, I.E.L.; et al. Acetaldehyde as an intermediate in the electroreduction of carbon monoxide to ethanol on oxide-derived copper. *Angew. Chem. Int. Ed.* **2016**, *55*, 1450–1454. [CrossRef]

54. Zhao, Z.; Zhang, Y.; Li, Y.; Zhao, H.; Quan, X. Electrochemical reduction of carbondioxide to formate with Fe-C electrodes in anaerobic sludge digestion process. *Water Res.* **2016**, *106*, 339–343. [CrossRef]

55. Lu, M.; Li, Q.; Liu, J.; Zhang, F.M.; Zhang, L.; Wang, J.L.; Kang, Z.H.; Lan, Y.Q. Installing earth-abundant metal active centers to covalent organic frameworks for efficient heterogeneous photocatalytic CO_2 reduction. *Appl. Catal. B Environ.* **2019**, *254*, 624–633. [CrossRef]

56. Swierk, J.R.; Mallouk, T.E. Design and development of photoanodes for water-splitting dye-sensitized photoelectrochemical cells. *Chem. Soc. Rev.* **2013**, *42*, 2357–2387. [CrossRef] [PubMed]

57. Todorova, T.K.; Huan, T.N.; Wang, X.; Agarwala, H.; Fontecave, M. Controlling hydrogen evolution during photoreduction of CO_2 to formic acid using [Rh(R-bpy)(Cp*)Cl](+) catalysts: A structure-activity study. *Inorg. Chem.* **2019**, *58*, 6893–6903. [CrossRef] [PubMed]

58. Chardon-Noblat, S.; Deronzier, A.; Ziessel, R.; Zsoldos, D. Electroreduction of CO_2 catalyzed by polymeric $[Ru(bpy)(CO)_2]_n$ films in aqueous media: Parameters influencing the reaction selectivity. *J. Electroanal. Chem.* **1998**, *444*, 253–260. [CrossRef]

59. Chen, J.; Yin, J.; Zheng, X.P.; Ahsaine, H.A.; Zhou, Y.; Dong, C.W.; Mohammed, O.F.; Takanabe, K.; Bakr, O.M. Compositionally screened eutectic catalytic coatings on halide perovskite photocathodes for photoassisted selective CO_2 reduction. *ACS Energy Lett.* **2019**, *4*, 1279–1286. [CrossRef]

60. Ajmal, S.; Yang, Y.; Li, K.J.; Tahir, M.A.; Liu, Y.Y.; Wang, T.; Bacha, A.U.R.; Feng, Y.Q.; Deng, Y.; Zhang, L.W. Zinc-modified copper catalyst for efficient (photo-) electrochemical CO_2 reduction with high selectivity of HCOOH production. *J. Phys. Chem. C* **2019**, *123*, 11555–11563. [CrossRef]

61. An, X.W.; Li, S.S.; Yoshida, A.; Wang, Z.D.; Hao, X.G.; Abudula, A.; Guan, G.Q. Electrodeposition of tin-based electrocatalysts with different surface tin species distributions for electrochemical reduction of CO_2 to HCOOH. *ACS Sustain. Chem. Eng.* **2019**, *7*, 9360–9368. [CrossRef]

62. Chatterjee, S.; Griego, C.; Hart, J.L.; Li, Y.W.; Taheri, M.L.; Keith, J.; Snyder, J.D. Free standing nanoporous palladium alloys as CO poisoning tolerant electrocatalysts for the electrochemical reduction of CO_2 to formate. *ACS Catal.* **2019**, *6*, 5290–5301. [CrossRef]

63. Raju, R.K.; Rodriguez, P.; Johnston, R.L. Can a single valence electron alter the electrocatalytic activity and selectivity for CO_2 reduction on the subnanometer scale? *J. Phys. Chem. C* **2019**, *123*, 14591–14609. [CrossRef]

64. Qin, C.L.; Fan, A.X.; Zhang, X.; Dai, X.P.; Sun, H.; Ren, D.H.; Dong, Z.; Wang, Y.; Luan, C.L.; Ye, J.Y.; et al. The in situ etching assisted synthesis of Pt-Fe-Mn ternary alloys with high-index facets as efficient catalysts for electro-oxidation reactions. *Nanoscale* **2019**, *11*, 9061–9075. [CrossRef]

65. Pan, F.P.; Li, B.Y.; Deng, W.; Du, Z.C.; Gang, Y.; Wang, G.F.; Li, Y. Promoting electrocatalytic CO_2 reduction on nitrogen-doped carbon with sulfur addition. *Appl. Catal. B Environ.* **2019**, *252*, 240–249. [CrossRef]

66. Yin, Y.; Gao, D.F.; Yao, S.Y.; Zhao, B.; Cai, F.; Lin, L.L.; Tang, P.; Zhai, P.; Wang, G.X.; Ma, D.; et al. Highly selective palladium-copper bimetallic electrocatalysts for the electrochemical reduction of CO_2 to CO. *Nano Energy* **2016**, *27*, 35–43. [CrossRef]

67. Gong, Q.F.; Ding, P.; Xu, M.Q.; Zhu, X.R.; Wang, M.Y.; Deng, J.; Ma, Q.; Han, N.; Zhu, Y.; Lu, J.; et al. Structural defects on converted bismuth oxide nanotubes enable highly active electrocatalysis of carbon dioxide reduction. *Nat. Comm.* **2019**, *10*, 2807. [CrossRef] [PubMed]

68. Gao, D.; Zhou, H.; Wang, J.; Miao, S.; Yang, F.; Wang, G.; Wang, J.; Bao, X. Size-dependent electrocatalytic reduction of CO_2 over Pd nanoparticles. *J. Am. Chem. Soc.* **2015**, *137*, 4288–4291. [CrossRef]

69. Jiang, B.; Zhang, X.G.; Jiang, K.; Wu, D.Y.; Cai, W.B. Boosting formate production in electrocatalytic CO_2 reduction over wide potential window on Pd surfaces. *J. Am. Chem. Soc.* **2018**, *140*, 2880–2889. [CrossRef] [PubMed]

70. Eder, G.M.; Pyles, D.A.; Wolfson, E.R.; McGrier, P.L. A ruthenium porphyrin-based porous organic polymer for the hydrosilylative reduction of CO_2 to formate. *Chem. Comm.* **2019**, *55*, 7195–7198. [CrossRef]

71. Weetman, C.; Bag, P.; Szilvasi, T.; Jandl, C.; Inoue, S. CO_2 Fixation and catalytic reduction by a neutral aluminum double bond. *Angew. Chem. Int. Ed.* **2019**, *58*, 10961–10965. [CrossRef]

72. Zhao, Y.; Wang, T.H.; Wang, Y.B.; Hao, R.L.; Wang, H.; Han, Y.H. Catalytic reduction of CO_2 to HCO_2^- by nanoscale nickel-based bimetallic alloy under atmospheric pressure. *J. Ind. Eng. Chem.* **2019**, *77*, 291–302. [CrossRef]

73. Porosoff, M.D.; Yan, B.; Chen, J.G. Catalytic reduction of CO_2 by H_2 for synthesis of CO, methanol and hydrocarbons: Challenges and opportunities. *Energy Environ. Sci.* **2016**, *9*, 62–73. [CrossRef]

74. Rodriguez, J.A.; Liu, P.; Stacchiola, D.J.; Senanayake, S.D.; White, M.G.; Chen, J.G. Hydrogenation of CO_2 to methanol: Importance of metal-oxide and metal-carbide interfaces in the activation of CO_2. *ACS Catal.* **2015**, *5*, 6696–6706. [CrossRef]

75. Gao, P.; Dang, S.; Li, S.; Bu, X.; Liu, Z.; Qiu, M.; Yang, C.; Wang, H.; Zhong, L.; Han, Y.; et al. Direct production of lower olefins from CO_2 conversion via bifunctional catalysis. *ACS Catal.* **2018**, *8*, 571–578. [CrossRef]

76. Sun, K.; Fan, Z.; Ye, J.; Yan, J.; Ge, Q.; Li, Y.; He, W.; Yang, W.; Liu, C. Hydrogenation of CO_2 to methanol over In_2O_3 catalyst. *J. CO_2 Util.* **2015**, *12*, 1–6. [CrossRef]

77. Gnanamani, M.K.; Jacobs, G.; Hamdeh, H.H.; Shafer, W.D.; Liu, F.; Hopps, S.D.; Thomas, G.A.; Davis, B.H. Hydrogenation of carbon dioxide over Co-Fe bimetallic catalysts. *ACS Catal.* **2016**, *6*, 913–927. [CrossRef]

78. Dreyer, J.A.H.; Li, P.; Zhang, L.; Beh, G.K.; Zhang, R.; Sit, P.H.L.; Teoh, W.Y. Influence of the oxide support reducibility on the CO_2 methanation over Ru-based catalysts. *Appl. Catal. B Environ.* **2017**, *219*, 715–726. [CrossRef]

79. Li, W.; Nie, X.; Jiang, X.; Zhang, A.; Ding, F.; Liu, M.; Liu, Z.; Guo, X.; Song, C. ZrO_2 support imparts superior activity and stability of Co catalysts for CO_2 methanation. *Appl. Catal. B Environ.* **2018**, *220*, 397–408. [CrossRef]

80. Zhan, G.; Zeng, H.C. ZIF-67-derived nanoreactors for controlling product selectivity in CO_2 hydrogenation. *ACS Catal.* **2017**, *7*, 7509–7519. [CrossRef]

81. Li, Y.; Cai, X.; Chen, S.; Zhang, H.; Zhang, K.H.L.; Hong, J.; Chen, B.; Kuo, D.H.; Wang, W. Highly dispersed metal carbide on ZIF-derived pyridinic-N-doped carbon for CO_2 enrichment and selective hydrogenation. *ChemSusChem* **2018**, *11*, 1040–1047. [CrossRef] [PubMed]

82. Kattel, S.; Yu, W.; Yang, X.; Yan, B.; Huang, Y.; Wan, W.; Liu, P.; Chen, J.G. CO_2 hydrogenation over oxide-supported PtCo catalysts: The role of the oxide support in determining the product selectivity. *Angew. Chem. Int. Ed.* **2016**, *55*, 7968–7973. [CrossRef]

83. Ren, J.; Qin, X.; Yang, J.Z.; Qin, Z.F.; Guo, H.L.; Lin, J.Y.; Li, Z. Methanation of carbon dioxide over Ni-M/ZrO_2 (M = Fe, Co, Cu) catalysts: Effect of addition of a second metal. *Fuel Process. Technol.* **2015**, *137*, 204–211. [CrossRef]

84. Kirchner, J.; Anolleck, J.K.; Loesch, H.; Kureti, S. Methanation of CO_2 on iron based catalysts. *Appl. Catal. B Environ.* **2018**, *223*, 47–59. [CrossRef]

85. Bi, Q.; Huang, X.; Yin, G.; Chen, T.; Du, X.; Cai, J.; Xu, J.; Liu, Z.; Han, Y.; Huang, F. Cooperative catalysis of nickel and nickel oxide for efficient reduction of CO_2 to CH_4. *ChemCatChem* **2019**, *11*, 1295–1302. [CrossRef]

86. Dietz, L.; Piccinin, S.; Maestri, M. Mechanistic insights into CO_2 activation via reverse water-gas shift on metal surfaces. *J. Phys. Chem. C* **2015**, *119*, 4959–4966. [CrossRef]

87. Kattel, S.; Yan, B.; Chen, J.G.; Liu, P. CO_2 hydrogenation on Pt, Pt/SiO_2 and Pt/TiO_2: Importance of synergy between Pt and oxide support. *J. Catal.* **2016**, *343*, 115–126. [CrossRef]

88. Yang, X.; Su, X.; Chen, X.; Duan, H.; Liang, B.; Liu, Q.; Liu, X.; Ren, Y.; Huang, Y.; Zhang, T. Promotion effects of potassium on the activity and selectivity of Pt/zeolite catalysts for reverse water gas shift reaction. *Appl. Catal. B Environ.* **2017**, *216*, 95–105. [CrossRef]

89. Wang, X.; Shi, H.; Kwak, J.H.; Szanyi, J. Mechanism of CO_2 hydrogenation on Pd/Al_2O_3 catalysts: Kinetics and transient DRIFTS-MS studies. *ACS Catal.* **2015**, *5*, 6337–6349. [CrossRef]

90. Guo, Y.; Mei, S.; Yuan, K.; Wang, D.J.; Liu, H.C.; Yan, C.H.; Zhang, Y.W. Low-temperature CO_2 methanation over CeO_2-supported Ru single atoms, nanoclusters, and nanoparticles competitively tuned by strong metal-support interactions and H-spillover effect. *ACS Catal.* **2018**, *8*, 6203–6215. [CrossRef]

91. Xu, J.; Su, X.; Duan, H.; Hou, B.; Lin, Q.; Liu, X.; Pan, X.; Pei, G.; Geng, H.; Huang, Y.; et al. Influence of pretreatment temperature on catalytic performance of rutile TiO_2-supported ruthenium catalyst in CO_2 methanation. *J. Catal.* **2016**, *333*, 227–237. [CrossRef]

92. Wu, H.C.; Chang, Y.C.; Wu, J.H.; Lin, J.H.; Lin, I.K.; Chen, C.S. Methanation of CO_2 and reverse water gas shift reactions on Ni/SiO_2 catalysts: The influence of particle size on selectivity and reaction pathway. *Catal. Sci. Technol.* **2015**, *5*, 4154–4163. [CrossRef]

93. Ren, H.; Xu, C.H.; Zhao, H.Y.; Wang, Y.X.; Liu, J.; Liu, J.Y. Methanol synthesis from CO_2 hydrogenation over Cu/gamma-Al_2O_3 catalysts modified by ZnO, ZrO_2 and MgO. *J. Ind. Eng. Chem.* **2015**, *28*, 261–267. [CrossRef]

94. Hus, M.; Dasireddy, V.D.B.C.; Stefancic, N.S.; Likozar, B. Mechanism, kinetics and thermodynamics of carbon dioxide hydrogenation to methanol on Cu/$ZnAl_2O_4$ spinel-type heterogeneous catalysts. *Appl. Catal. B Environ.* **2017**, *207*, 267–278. [CrossRef]

95. Studt, F.; Behrens, M.; Kunkes, E.L.; Thomas, N.; Zander, S.; Tarasov, A.; Schumann, J.; Frei, E.; Varley, J.B.; Abild-Pedersen, F.; et al. The mechanism of CO and CO_2 hydrogenation to methanol over Cu-based catalysts. *ChemCatChem* **2015**, *7*, 1105–1111. [CrossRef]

96. Kunkes, E.L.; Studt, F.; Abild-Pedersen, F.; Schloegl, R.; Behrens, M. Hydrogenation of CO_2 to methanol and CO on Cu/ZnO/Al_2O_3: Is there a common intermediate or not? *J. Catal.* **2015**, *328*, 43–48. [CrossRef]

97. Karelovic, A.; Ruiz, P. The role of copper particle size in low pressure methanol synthesis via CO_2 hydrogenation over Cu/ZnO catalysts. *Catal. Sci. Technol.* **2015**, *5*, 869–881. [CrossRef]

98. Ro, I.; Liu, Y.; Ball, M.R.; Jackson, D.H.K.; Chada, J.P.; Sener, C.; Kuech, T.F.; Madon, R.J.; Huber, G.W.; Dumesic, J.A. Role of the Cu-ZrO_2 interfacial sites for conversion of ethanol to ethyl acetate and synthesis of methanol from CO_2 and H_2. *ACS Catal.* **2016**, *6*, 7040–7050. [CrossRef]

99. Phongamwong, T.; Chantaprasertporn, U.; Witoon, T.; Numpilai, T.; Poo-Arporn, Y.; Limphirat, W.; Donphai, W.; Dittanet, P.; Chareonpanich, M.; Limtrakul, J. CO_2 hydrogenation to methanol over CuO-ZnO-ZrO_2-SiO_2 catalysts: Effects of SiO_2 contents. *Chem. Eng. J.* **2017**, *316*, 692–703. [CrossRef]

100. Jiang, X.; Koizumi, N.; Guo, X.; Song, C. Bimetallic Pd-Cu catalysts for selective CO_2 hydrogenation to methanol. *Appl. Catal. B Environ.* **2015**, *170*, 173–185. [CrossRef]

101. Bahruji, H.; Bowker, M.; Hutchings, G.; Dimitratos, N.; Wells, P.; Gibson, E.; Jones, W.; Brookes, C.; Morgan, D.; Lalev, G. Pd/ZnO catalysts for direct CO_2 hydrogenation to methanol. *J. Catal.* **2016**, *343*, 133–146. [CrossRef]

102. Nie, X.; Jiang, X.; Wang, H.; Luo, W.; Janik, M.J.; Chen, Y.; Guo, X.; Song, C. Mechanistic understanding of alloy effect and water promotion for Pd-Cu bimetallic catalysts in CO_2 hydrogenation to methanol. *ACS Catal.* **2018**, *8*, 4873–4892. [CrossRef]

103. Stangeland, K.; Kalai, D.Y.; Ding, Y.; Yu, Z. Mesoporous manganese-cobalt oxide spinel catalysts for CO_2 hydrogenation to methanol. *J. CO_2 Util.* **2019**, *32*, 146–154. [CrossRef]

104. Martin, O.; Martín, A.J.; Mondelli, C.; Mitchell, S.; Segawa, T.F.; Hauert, R.; Drouilly, C.; Curulla-Ferré, D.; Pérez-Ramírez, J. Indium oxide as a superior catalyst for methanol synthesis by CO_2 Hydrogenation. *Angew. Chem. Int. Ed.* **2016**, *55*, 6261–6265. [CrossRef]

105. Wei, J.; Ge, Q.; Yao, R.; Wen, Z.; Fang, C.; Guo, L.; Xu, H.; Sun, J. Directly converting CO_2 into a gasoline fuel. *Nat. Comm.* **2017**, *8*, 15174. [CrossRef]

106. Visconti, C.G.; Martinelli, M.; Falbo, L.; Infantes-Molina, A.; Lietti, L.; Forzatti, P.; Iaquaniello, G.; Palo, E.; Picutti, B.; Brignoli, F. CO_2 hydrogenation to lower olefins on a high surface area K-promoted bulk Fe-catalyst. *Appl. Catal. B Environ.* **2017**, *200*, 530–542. [CrossRef]

107. Albrecht, M.; Rodemerck, U.; Schneider, M.; Broering, M.; Baabe, D.; Kondratenko, E.V. Unexpectedly efficient CO_2 hydrogenation to higher hydrocarbons over non-doped Fe_2O_3. *Appl. Catal. B Environ.* **2017**, *204*, 119–126. [CrossRef]

108. Liu, J.; Zhang, A.; Liu, M.; Hu, S.; Ding, F.; Song, C.; Guo, X. Fe-MOF-derived highly active catalysts for carbon dioxide hydrogenation to valuable hydrocarbons. *J. CO_2 Util.* **2017**, *21*, 100–107. [CrossRef]

109. Choi, Y.H.; Jang, Y.J.; Park, H.; Kim, W.Y.; Lee, Y.H.; Choi, S.H.; Lee, J.S. Carbon dioxide Fischer-Tropsch synthesis: A new path to carbon-neutral fuels. *Appl. Catal. B Environ.* **2017**, *202*, 605–610. [CrossRef]

110. Wei, J.; Sun, J.; Wen, Z.; Fang, C.; Ge, Q.; Xu, H. New insights into the effect of sodium on Fe_3O_4-based nanocatalysts for CO_2 hydrogenation to light olefins. *Catal. Sci. Technol.* **2016**, *6*, 4786–4793. [CrossRef]

111. Satthawong, R.; Koizumi, N.; Song, C.; Prasassarakich, P. Light olefin synthesis from CO_2 hydrogenation over K-promoted Fe-Co bimetallic catalysts. *Catal. Today* **2015**, *251*, 34–40. [CrossRef]

112. Gao, P.; Li, S.; Bu, X.; Dang, S.; Liu, Z.; Wang, H.; Zhong, L.; Qiu, M.; Yang, C.; Cai, J.; et al. Direct conversion of CO_2 into liquid fuels with high selectivity over a bifunctional catalyst. *Nat. Chem.* **2017**, *9*, 1019–1024. [CrossRef]

113. Cheah, W.Y.; Show, P.L.; Chang, J.S.; Ling, T.C.; Juan, J.C. Biosequestration of atmospheric CO_2 and flue gas-containing CO_2 by microalgae. *Bioresour. Technol.* **2015**, *184*, 190–201. [CrossRef] [PubMed]

114. Yadav, G.; Sen, R. Microalgal green refinery concept for biosequestration of carbon-dioxide vis-à-vis wastewater remediation and bioenergy production: Recent technological advances in climate research. *J. CO_2 Util.* **2017**, *17*, 188–206. [CrossRef]

115. Kuo, C.M.; Jian, J.F.; Sun, Y.L.; Lin, T.H.; Yang, Y.C.; Zhang, W.X.; Chang, H.F.; Lai, J.T.; Chang, J.S.; Lin, C.S. An efficient photobioreactors/raceway circulating system combined with alkaline-CO_2 capturing medium for microalgal cultivation. *Bioresour. Technol.* **2018**, *266*, 398–406. [CrossRef] [PubMed]

116. Duan, Y.; Shi, F. Bioreactor design for algal growth as a sustainable energy source. In *Reactor and Process Design in Sustainable Energy Technology*; Elsevier: Amsterdam, The Netherlands, 2014; pp. 27–60.

117. Xie, Y.P.; Ho, S.H.; Chen, C.Y.; Chen, C.N.N.; Liu, C.C.; Ng, I.S.; Jing, K.J.; Yang, S.C.; Chen, C.H.; Chang, J.S.; et al. Simultaneous enhancement of CO_2 fixation and lutein production with thermo-tolerant *Desmodesmus* sp. F51 using a repeated fed-batch cultivation strategy. *Biochem. Eng. J.* **2014**, *86*, 33–40. [CrossRef]

118. Gonçalves, A.L.; Rodrigues, C.M.; Pires, J.C.M.; Simões, M. The effect of increasing CO_2 concentrations on its capture, biomass production and wastewater bioremediation by microalgae and cyanobacteria. *Algal Res.* **2016**, *14*, 127–136. [CrossRef]

119. Chen, H.; Wang, J.; Zheng, Y.; Zhan, J.; He, C.; Wang, Q. Algal biofuel production coupled bioremediation of biomass power plant wastes based on *Chlorella* sp C2 cultivation. *Appl. Energy* **2018**, *211*, 296–305. [CrossRef]

120. Jain, D.; Ghonse, S.S.; Trivedi, T.; Fernandes, G.L.; Menezes, L.D.; Damare, S.R.; Mamatha, S.S.; Kumar, S.; Gupta, V. CO_2 fixation and production of biodiesel by *Chlorella vulgaris* NIOCCV under mixotrophic cultivation. *Bioresour. Technol.* **2019**, *273*, 672–676. [CrossRef]

121. Kumar, K.; Banerjee, D.; Das, D. Carbon dioxide sequestration from industrial flue gas by *Chlorella sorokiniana*. *Bioresour. Technol.* **2014**, *152*, 225–233. [CrossRef]

122. Tripathi, R.; Singh, J.; Thakur, I.S. Characterization of microalga *Scenedesmus* sp ISTGA1 for potential CO_2 sequestration and biodiesel production. *Renew. Energy* **2015**, *74*, 774–781. [CrossRef]

123. Varshney, P.; Beardall, J.; Bhattacharya, S.; Wangikar, P.P. Isolation and biochemical characterisation of two thermophilic green algal species- *Asterarcys quadricellulare* and *Chlorella sorokiniana*, which are tolerant to high levels of carbon dioxide and nitric oxide. *Algal Res.* **2018**, *30*, 28–37. [CrossRef]

124. Yun, H.S.; Ji, M.K.; Park, Y.T.; Salama, E.S.; Choi, J. Microalga, *Acutodesmus obliquus* KGE 30 as a potential candidate for CO_2 mitigation and biodiesel production. *Environ. Sci. Pollut. Res.* **2016**, *23*, 17831–17839. [CrossRef]

125. Bhakta, J.N.; Lahiri, S.; Pittman, J.K.; Jana, B.B. Carbon dioxide sequestration in wastewater by a consortium of elevated carbon dioxide-tolerant microalgae. *J. CO_2 Util.* **2015**, *10*, 105–112. [CrossRef]

126. Kuo, C.M.; Lin, T.H.; Yang, Y.C.; Zhang, W.X.; Lai, J.T.; Wu, H.T.; Chang, J.S.; Lin, C.S. Ability of an alkali-tolerant mutant strain of the microalga *Chlorella* sp. AT1 to capture carbon dioxide for increasing carbon dioxide utilization efficiency. *Bioresour. Technol.* **2017**, *244*, 243–251. [CrossRef] [PubMed]

127. Yang, B.; Liu, J.; Ma, X.; Guo, B.; Liu, B.; Wu, T.; Jiang, Y.; Chen, F. Genetic engineering of the Calvin cycle toward enhanced photosynthetic CO_2 fixation in microalgae. *Biotechnol. Biofuels* **2017**, *10*, 229. [CrossRef] [PubMed]

128. Li, D.; Wang, L.; Zhao, Q.; Wei, W.; Sun, Y. Improving high carbon dioxide tolerance and carbon dioxide fixation capability of *Chlorella* sp by adaptive laboratory evolution. *Bioresour. Technol.* **2015**, *185*, 269–275. [CrossRef]

129. Bilanovic, D.; Holland, M.; Starosvetsky, J.; Armon, R. Co-cultivation of microalgae and nitrifiers for higher biomass production and better carbon capture. *Bioresour. Technol.* **2016**, *220*, 282–288. [CrossRef]

130. Aslam, A.; Thomas-Hall, S.R.; Mughal, T.A.; Schenk, P.M. Selection and adaptation of microalgae to growth in 100% unfiltered coal-fired flue gas. *Bioresour. Technol.* **2017**, *233*, 271–283. [CrossRef] [PubMed]

131. Nayak, M.; Suh, W.I.; Lee, B.; Chang, Y.K. Enhanced carbon utilization efficiency and FAME production of *Chlorella* sp HS2 through combined supplementation of bicarbonate and carbon dioxide. *Energy Convers. Manag.* **2018**, *156*, 45–52. [CrossRef]

132. Jiang, Y.; Zhang, W.; Wang, J.; Chen, Y.; Shen, S.; Liu, T. Utilization of simulated flue gas for cultivation of *Scenedesmus dimorphus*. *Bioresour. Technol.* **2013**, *128*, 359–364. [CrossRef]

133. Vo, H.N.P.; Bui, X.T.; Nguyen, T.T.; Nguyen, D.D.; Dao, T.S.; Cao, N.D.T.; Vo, T.K.Q. Effects of nutrient ratios and carbon dioxide bio-sequestration on biomass growth of *Chlorella* sp in bubble column photobioreactor. *J. Environ. Manag.* **2018**, *219*, 1–8. [CrossRef]

134. Liu, X.; Ying, K.; Chen, G.; Zhou, C.; Zhang, W.; Zhang, X.; Cai, Z.; Holmes, T.; Tao, Y. Growth of *Chlorella vulgaris* and nutrient removal in the wastewater in response to intermittent carbon dioxide. *Chemosphere* **2017**, *186*, 977–985. [CrossRef]

135. Posadas, E.; Morales, M.d.M.; Gomez, C.; Acién, F.G.; Muñoz, R. Influence of pH and CO_2 source on the performance of microalgae-based secondary domestic wastewater treatment in outdoors pilot raceways. *Chem. Eng. J.* **2015**, *265*, 239–248. [CrossRef]

136. Kuo, C.M.; Jian, J.F.; Lin, T.H.; Chang, Y.B.; Wan, X.H.; Lai, J.T.; Chang, J.S.; Lin, C.S. Simultaneous microalgal biomass production and CO_2 fixation by cultivating *Chlorella* sp. GD with aquaculture wastewater and boiler flue gas. *Bioresour. Technol.* **2016**, *221*, 241–250. [CrossRef]

137. Eze, V.C.; Velasquez-Orta, S.B.; Hernandez-Garcia, A.; Monje-Ramirez, I.; Orta-Ledesma, M.T. Kinetic modelling of microalgae cultivation for wastewater treatment and carbon dioxide sequestration. *Algal Res.* **2018**, *32*, 131–141. [CrossRef]

138. Fu, W.; Gudmundsson, S.; Wichuk, K.; Palsson, S.; Palsson, B.O.; Salehi-Ashtiani, K.; Brynjolfsson, S. Sugar-stimulated CO_2 sequestration by the green microalga *Chlorella vulgaris*. *Sci. Total Environ.* **2019**, *654*, 275–283. [CrossRef]

139. Dineshkumar, R.; Subramanian, G.; Dash, S.K.; Sen, R. Development of an optimal light-feeding strategy coupled with semi-continuous reactor operation for simultaneous improvement of microalgal photosynthetic efficiency, lutein production and CO_2 sequestration. *Biochem. Eng. J.* **2016**, *113*, 47–56. [CrossRef]

140. Jacob-Lopes, E.; Franco, T.T. From oil refinery to microalgal biorefinery. *J. CO_2 Util.* **2013**, *2*, 1–7. [CrossRef]

141. Kassim, M.A.; Meng, T.K. Carbon dioxide (CO_2) biofixation by microalgae and its potential for biorefinery and biofuel production. *Sci. Total Environ.* **2017**, *584*, 1121–1129. [CrossRef]

142. Kao, C.Y.; Chen, T.Y.; Chang, Y.B.; Chiu, T.W.; Lin, H.Y.; Chen, C.D.; Chang, J.S.; Lin, C.S. Utilization of carbon dioxide in industrial flue gases for the cultivation of microalga *Chlorella* sp. *Bioresour. Technol.* **2014**, *166*, 485–493. [CrossRef] [PubMed]

143. Huang, Y.; Sun, Y.; Liao, Q.; Fu, Q.; Xia, A.; Zhu, X. Improvement on light penetrability and microalgae biomass production by periodically pre-harvesting *Chlorella vulgaris* cells with culture medium recycling. *Bioresour. Technol.* **2016**, *216*, 669–676. [CrossRef]

144. Moheimani, N.R. *Tetraselmis suecica* culture for CO_2 bioremediation of untreated flue gas from a coal-fired power station. *J. Appl. Phycol.* **2016**, *28*, 2139–2146. [CrossRef]

145. Ou-Yang, C.; Chen, H.W.; Ho, C.H.; Chou, J.C.; Yuan, Y.T.; Ho, C.L.; Hsueh, H.T.; Chen, S.T.; Liao, P.C.; Chao, L.K. Value chain analysis of algal bioenergy and carbon capture integrated with a biotechnology innovation. *J. Clean. Prod.* **2018**, *180*, 349–359. [CrossRef]

146. Zhu, L.D.; Xu, Z.B.; Qin, L.; Wang, Z.M.; Hiltunen, E.; Li, Z.H. Oil production from pilot-scale microalgae cultivation: An economics evaluation. *Energy Sources Part B Econ. Plan. Policy* **2016**, *11*, 11–17. [CrossRef]

147. Rezvani, S.; Moheimani, N.R.; Bahri, P.A. Techno-economic assessment of CO_2 bio-fixation using microalgae in connection with three different state-of-the-art power plants. *Comput. Chem. Eng.* **2016**, *84*, 290–301. [CrossRef]

148. Venkata Mohan, S.; Modestra, J.A.; Amulya, K.; Butti, S.K.; Velvizhi, G. A circular bioeconomy with biobased products from CO_2 sequestration. *Trends Biotechnol.* **2016**, *34*, 506–519. [CrossRef] [PubMed]

149. Chew, K.W.; Yap, J.Y.; Show, P.L.; Suan, N.H.; Juan, J.C.; Ling, T.C.; Lee, D.J.; Chang, J.S. Microalgae biorefinery: High value products perspectives. *Bioresour. Technol.* **2017**, *229*, 53–62. [CrossRef]

150. Duque-Acevedo, M.; Belmonte-Ureña, L.J.; Plaza-Úbeda, J.A.; Camacho-Ferre, F. The management of agricultural waste biomass in the framework of circular economy and bioeconomy: An opportunity for greenhouse agriculture in southeast Spain. *Agronomy* **2020**, *10*, 489. [CrossRef]

151. Dębowski, M.; Zieliński, M.; Kazimierowicz, J.; Kujawska, N.; Talbierz, S. Microalgae cultivation technologies as an opportunity for bioenergetic system development—Advantages and limitations. *Sustainability* **2020**, *12*, 9980. [CrossRef]

152. Khan, M.I.; Shin, J.H.; Kim, J.D. The promising future of microalgae: Current status, challenges, and optimization of a sustainable and renewable industry for biofuels, feed, and other products. *Microb. Cell Factories* **2018**, *17*, 36. [CrossRef]

153. Alobwede, E.; Leake, J.R.; Pandhal, J. Circular economy fertilization: Testing micro and macro algal species as soil improvers and nutrient sources for crop production in greenhouse and field conditions. *Geoderma* **2019**, *334*, 113–123. [CrossRef]

154. Sprague, M.; Dick, J.R.; Tocher, D.R. Impact of sustainable feeds on omega-3 long-chain fatty acid levels in farmed Atlantic salmon, 2006–2015. *Sci. Rep.* **2016**, *6*, 21892. [CrossRef] [PubMed]

155. Dineshbabu, G.; Goswami, G.; Kumar, R.; Sinha, A.; Das, D. Microalgae—Nutritious, sustainable aqua- and animal feed source. *J. Funct. Foods* **2019**, *62*, 103545. [CrossRef]

156. Shakya, R.; Whelen, J.; Adhikari, S.; Mahadevan, R.; Neupane, S. Effect of temperature and Na$_2$CO$_3$ catalyst on hydrothermal liquefaction of algae. *Algal Res.* **2015**, *12*, 80–90. [CrossRef]

157. Gai, C.; Zhang, Y.; Chen, W.T.; Zhang, P.; Dong, Y. An investigation of reaction pathways of hydrothermal liquefaction using *Chlorella pyrenoidosa* and *Spirulina platensis*. *Energy Convers. Manag.* **2015**, *96*, 330–339. [CrossRef]

158. Chen, Y.; Mu, R.; Yang, M.; Fang, L.; Wu, Y.; Wu, K.; Liu, Y.; Gong, J. Catalytic hydrothermal liquefaction for bio-oil production over CNTs supported metal catalysts. *Chem. Eng. Sci.* **2017**, *161*, 299–307. [CrossRef]

159. López Barreiro, D.; Bauer, M.; Hornung, U.; Posten, C.; Kruse, A.; Prins, W. Cultivation of microalgae with recovered nutrients after hydrothermal liquefaction. *Algal Res.* **2015**, *9*, 99–106. [CrossRef]

160. Chen, W.H.; Lin, B.J.; Huang, M.Y.; Chang, J.S. Thermochemical conversion of microalgal biomass into biofuels: A review. *Bioresour. Technol.* **2015**, *184*, 314–327. [CrossRef] [PubMed]

161. Raheem, A.; Dupont, V.; Channa, A.Q.; Zhao, X.; Vuppaladadiyam, A.K.; Taufiq-Yap, Y.H.; Zhao, M.; Harun, R. Parametric characterization of air gasification of *Chlorella vulgaris* biomass. *Energy Fuels* **2017**, *31*, 2959–2969. [CrossRef]

162. Tiong, L.; Komiyama, M.; Uemura, Y.; Nguyen, T.T. Catalytic supercritical water gasification of microalgae: Comparison of *Chlorella vulgaris* and *Scenedesmus quadricauda*. *J. Supercrit. Fluids* **2016**, *107*, 408–413. [CrossRef]

163. Peng, G.; Vogel, F.; Refardt, D.; Ludwig, C. Catalytic supercritical water gasification: Continuous methanization of *Chlorella vulgaris*. *Ind. Eng. Chem. Res.* **2017**, *56*, 6256–6265. [CrossRef]

164. Hu, Z.; Ma, X.; Jiang, E. The effect of microwave pretreatment on chemical looping gasification of microalgae for syngas production. *Energy Convers. Manag.* **2017**, *143*, 513–521. [CrossRef]

165. Liu, G.; Liao, Y.; Wu, Y.; Ma, X. Synthesis gas production from microalgae gasification in the presence of Fe$_2$O$_3$ oxygen carrier and CaO additive. *Appl. Energy* **2018**, *212*, 955–965. [CrossRef]

166. Azizi, K.; Keshavarz Moraveji, M.; Abedini Najafabadi, H. A review on bio-fuel production from microalgal biomass by using pyrolysis method. *Renew. Sustain. Energy Rev.* **2018**, *82*, 3046–3059. [CrossRef]

167. Wang, X.; Sheng, L.; Yang, X. Pyrolysis characteristics and pathways of protein, lipid and carbohydrate isolated from microalgae *Nannochloropsis* sp. *Bioresour. Technol.* **2017**, *229*, 119–125. [CrossRef] [PubMed]

168. Lu, Q.; Guo, H.; Zhou, M.; Cui, M.; Dong, C.; Yang, Y. Selective preparation of monocyclic aromatic hydrocarbons from catalytic cracking of biomass fast pyrolysis vapors over Mo$_2$N/HZSM-5 catalyst. *Fuel Process. Technol.* **2018**, *173*, 134–142. [CrossRef]

169. Zainan, N.H.; Srivatsa, S.C.; Li, F.; Bhattacharya, S. Quality of bio-oil from catalytic pyrolysis of microalgae *Chlorella vulgaris*. *Fuel* **2018**, *223*, 12–19. [CrossRef]

170. Zabed, H.M.; Qi, X.; Yun, J.; Zhang, H. Anaerobic digestion of microalgae biomass for methane production. In *Microalgae Biotechnology for Development of Biofuel and Wastewater Treatment*; Alam, M.A., Wang, Z., Eds.; Springer: Singapore, 2019; pp. 397–421.

171. Wang, Y.; Guo, W.; Cheng, C.L.; Ho, S.H.; Chang, J.S.; Ren, N. Enhancing bio-butanol production from biomass of *Chlorella vulgaris* JSC-6 with sequential alkali pretreatment and acid hydrolysis. *Bioresour. Technol.* **2016**, *200*, 557–564. [CrossRef]

172. Abomohra, A.E.F.; Elshobary, M. Biodiesel, bioethanol, and biobutanol production from microalgae. In *Microalgae Biotechnology for Development of Biofuel and Wastewater Treatment*; Alam, M.A., Wang, Z., Eds.; Springer: Singapore, 2019; pp. 293–321.

173. Passos, F.; Carretero, J.; Ferrer, I. Comparing pretreatment methods for improving microalgae anaerobic digestion: Thermal, hydrothermal, microwave and ultrasound. *Chem. Eng. J.* **2015**, *279*, 667–672. [CrossRef]

174. Bohutskyi, P.; Betenbaugh, M.J.; Bouwer, E.J. The effects of alternative pretreatment strategies on anaerobic digestion and methane production from different algal strains. *Bioresour. Technol.* **2014**, *155*, 366–372. [CrossRef]

175. Passos, F.; Hom-Diaz, A.; Blanquez, P.; Vicent, T.; Ferrer, I. Improving biogas production from microalgae by enzymatic pretreatment. *Bioresour. Technol.* **2016**, *199*, 347–351. [CrossRef]

176. Hernandez, D.; Riano, B.; Coca, M.; Garcia-Gonzalez, M.C. Saccharification of carbohydrates in microalgal biomass by physical, chemical and enzymatic pre-treatments as a previous step for bioethanol production. *Chem. Eng. J.* **2015**, *262*, 939–945. [CrossRef]

177. Shokrkar, H.; Ebrahimi, S.; Zamani, M. Bioethanol production from acidic and enzymatic hydrolysates of mixed microalgae culture. *Fuel* **2017**, *200*, 380–386. [CrossRef]

178. Cheng, L.M.; Lee, K.T.; Chan, D.J.C. Synergistic effect of pretreatment and fermentation process on carbohydrate-rich Scenedesmus dimorphus for bioethanol production. *Energy Convers. Manag.* **2017**, *141*, 410–419. [CrossRef]

179. Dickinson, S.; Mientus, M.; Frey, D.; Amini-Hajibashi, A.; Ozturk, S.; Shaikh, F.; Sengupta, D.; El-Halwagi, M.M. A review of biodiesel production from microalgae. *Clean Technol. Environ. Policy* **2017**, *19*, 637–668. [CrossRef]

180. Jeevan Kumar, S.P.; Vijay Kumar, G.; Dash, A.; Scholz, P.; Banerjee, R. Sustainable green solvents and techniques for lipid extraction from microalgae: A review. *Algal Res.* **2017**, *21*, 138–147. [CrossRef]

181. Lai, Y.S.; De Francesco, F.; Aguinaga, A.; Parameswaran, P.; Rittmann, B.E. Improving lipid recovery from *Scenedesmus* wet biomass by surfactant-assisted disruption. *Green Chem.* **2016**, *18*, 1319–1326. [CrossRef]

182. Orr, V.C.A.; Plechkova, N.V.; Seddon, K.R.; Rehmann, L. Disruption and wet extraction of the microalgae *Chlorella vulgaris* using room-temperature ionic liquids. *ACS Sustain. Chem. Eng.* **2016**, *4*, 591–600. [CrossRef]

183. Lee, O.K.; Oh, Y.K.; Lee, E.Y. Bioethanol production from carbohydrate-enriched residual biomass obtained after lipid extraction of *Chlorella* sp. KR-1. *Bioresour. Technol.* **2015**, *196*, 22–27. [CrossRef]

184. El-Dalatony, M.M.; Salama, E.S.; Kurade, M.B.; Kim, K.Y.; Govindwar, S.P.; Kim, J.R.; Kwon, E.E.; Min, B.; Jang, M.; Oh, S.E.; et al. Whole conversion of microalgal biomass into biofuels through successive high-throughput fermentation. *Chem. Eng. J.* **2019**, *360*, 797–805. [CrossRef]

185. Chen, C.Y.; Liu, C.C. Optimization of lutein production with a two-stage mixotrophic cultivation system with *Chlorella sorokiniana* MB-1. *Bioresour. Technol.* **2018**, *262*, 74–79. [CrossRef]

186. Xie, Y.; Zhao, X.; Chen, J.; Yang, X.; Ho, S.H.; Wang, B.; Chang, J.S.; Shen, Y. Enhancing cell growth and lutein productivity of *Desmodesmus* sp F51 by optimal utilization of inorganic carbon sources and ammonium salt. *Bioresour. Technol.* **2017**, *244*, 664–671. [CrossRef] [PubMed]

187. European Commission. *Communication from the Commission to the European Parliament, the Council, the European Economic and Social Committee and the Committee of the Regions. Closing the Loop—An EU Action Plan for the Circular Economy*; European Commission: Brussels, Belgium, 2015.

188. Bertolucci Paes, L.A.; Bezerra, B.S.; Deus, R.M.; Jugend, D.; Gomes Battistelle, R.A. Organic solid waste management in a circular economy perspective—A systematic review and SWOT analysis. *J. Clean. Prod.* **2019**, *239*, 118086. [CrossRef]

189. Teigiserova, D.A.; Hamelin, L.; Thomsen, M. Review of high-value food waste and food residues biorefineries with focus on unavoidable wastes from processing. *Resour. Conserv. Recycl.* **2019**, *149*, 413–426. [CrossRef]

190. Cao, Y.; Chen, S.S.; Zhang, S.C.; Ok, Y.S.; Matsagar, B.M.; Wu, K.C.W.; Tsang, D.C.W. Advances in lignin valorization towards bio-based chemicals and fuels: Lignin biorefinery. *Bioresour. Technol.* **2019**, *291*, 121878. [CrossRef] [PubMed]

191. Mitra, M.; Mishra, S. Multiproduct biorefinery from Arthrospira spp. towards zero waste: Current status and future trends. *Bioresour. Technol.* **2019**, *291*, 121928. [CrossRef] [PubMed]

192. Hemalatha, M.; Sarkar, O.; Mohan, S.V. Self-sustainable azolla-biorefinery platform for valorization of biobased products with circular-cascading design. *Chem. Eng. J.* **2019**, *373*, 1042–1053. [CrossRef]

193. Milledge, J.J.; Nielsen, B.V.; Maneein, S.; Harvey, P.J. A brief review of anaerobic digestion of algae for bioenergy. *Energies* **2019**, *12*, 1166. [CrossRef]

194. Abomohra, A.E.; Zheng, X.; Wang, Q.; Huang, J.; Ebaid, R. Enhancement of biodiesel yield and characteristics through in-situ solvo-thermal co-transesterification of wet microalgae with spent coffee grounds. *Bioresour. Technol.* **2021**, *323*, 124640. [CrossRef]

195. Ma, X.; Zheng, H.; Addy, M.; Anderson, E.; Liu, Y.; Chen, P.; Ruan, R. Cultivation of Chlorella vulgaris in wastewater with waste glycerol: Strategies for improving nutrients removal and enhancing lipid production. *Bioresour. Technol.* **2016**, *207*, 252–261. [CrossRef]

196. Abomohra, A.E.F.; Eladel, H.; El-Esawi, M.; Wang, S.; Wang, Q.; He, Z.X.; Feng, Y.Q.; Shang, H.; Hanelt, D. Effect of lipid-free microalgal biomass and waste glycerol on growth and lipid production of Scenedesmus obliquus: Innovative waste recycling for extraordinary lipid production. *Bioresour. Technol.* **2018**, *249*, 992–999. [CrossRef]

197. Yarnold, J.; Karan, H.; Oey, M.; Hankamer, B. Microalgal Aquafeeds as Part of a Circular Bioeconomy. *Trends Plant Sci.* **2019**, *24*, 959–970. [CrossRef] [PubMed]

198. Chew, K.W.; Chia, S.R.; Yen, H.W.; Nomanbhay, S.; Ho, Y.C.; Show, P.L. Transformation of biomass waste into sustainable organic fertilizers. *Sustainability* **2019**, *11*, 2266. [CrossRef]

199. Abad-Segura, E.; De La Fuente, A.B.; González-Zamar, M.; Belmonte-Ureña, L.J. Effects of circular economy policies on the environment and sustainable growth: Worldwide research. *Sustainability* **2020**, *12*, 5792. [CrossRef]